

## 7.05 Numerical Methods for Mantle Convection

**S. J. Zhong**, University of Colorado, Boulder, CO, USA

**D. A. Yuen**, University of Minnesota, Minneapolis, MN, USA

**L. N. Moresi**, Monash University, Clayton, VIC, Australia

© 2007 Elsevier B.V. All rights reserved.

---

<b>7.05.1</b>	<b>Introduction</b>	227
<b>7.05.2</b>	<b>Governing Equations and Initial and Boundary Conditions</b>	228
<b>7.05.3</b>	<b>Finite-Difference, Finite-Volume, and Spectral Methods</b>	229
7.05.3.1	Finite Difference	229
7.05.3.1.1	FD implementation of the governing equations	229
7.05.3.1.2	Approximations of spatial derivatives and solution approaches	230
7.05.3.2	FV Method	232
7.05.3.3	Spectral Methods	233
<b>7.05.4</b>	<b>An FE Method</b>	234
7.05.4.1	Stokes Flow: A Weak Formulation, Its FE Implementation, and Solution	234
7.05.4.1.1	A weak formulation	234
7.05.4.1.2	An FE implementation	236
7.05.4.1.3	The Uzawa algorithm for the matrix equation	238
7.05.4.1.4	Multigrid solution strategies	239
7.05.4.2	Stokes Flow: A Penalty Formulation	241
7.05.4.3	The SUPG Formulation for the Energy Equation	242
<b>7.05.5</b>	<b>Incorporating More Realistic Physics</b>	244
7.05.5.1	Thermochemical Convection	244
7.05.5.1.1	Governing equations	244
7.05.5.1.2	Solution approaches	244
7.05.5.2	Solid-State Phase Transition	246
7.05.5.3	Non-Newtonian Rheology	247
<b>7.05.6</b>	<b>Concluding Remarks and Future Prospects</b>	247
<b>References</b>		249

---

### 7.05.1 Introduction

The governing equations for mantle convection are derived from conservation laws of mass, momentum, and energy. The nonlinear nature of mantle rheology with its strong temperature and stress dependence and nonlinear coupling between flow velocity and temperature in the energy equation require that numerical methods be used to solve these governing equations. Understanding the dynamical effects of phase transitions (e.g., olivine-to-spinel phase transition) and multicomponent flow also demands numerical methods. Numerical modeling of mantle convection has a rich history since the late 1960s (e.g., Torrance and Turcotte, 1971; McKenzie *et al.*, 1974). Great progress in computer architecture along with improved numerical techniques has helped advance

the field of mantle convection into its own niche in geophysical fluid dynamics (e.g., Yuen *et al.*, 2000).

In this chapter, we will present several commonly used numerical methods in studies of mantle convection with the primary aim of reaching out to students and new researchers in the field. First, we will present the governing equations and the boundary and initial conditions for a given problem in mantle convection, and discuss the general efficient strategy to solve this problem numerically (Section 7.05.2). We will then briefly discuss finite-difference (FD), finite-volume (FV), and spectral methods in Section 7.05.3. Since finite elements (FEs) have attained very high popularity in the user community, we will discuss FEs in greater details as the most basic numerical tool (Section 7.05.4). For simplicity and clarity, we will focus our discussion on homogeneous,

incompressible fluids with the Boussinesq approximation. However, we will also describe methods for more complicated and realistic mantle situations by including non-Newtonian rheology, solid-state phase transitions, and thermochemical (i.e., multicomponent) convection (Section 7.05.5). Finally, in Section 7.05.6, we will discuss some new developments in computational sciences, such as software development and visualization, which may impact our future studies of mantle convection modeling.

## 7.05.2 Governing Equations and Initial and Boundary Conditions

The simplest mathematical formulation for mantle convection assumes incompressibility and the Boussinesq approximation (e.g., McKenzie *et al.*, 1974). Under this formulation, the nondimensional conservation equations of the mass, momentum, and energy are (*see* Chapter 7.02):

$$u_{i,i} = 0 \quad [1]$$

$$\sigma_{ij,j} + RaT\delta_{i3} = 0 \quad [2]$$

$$\frac{\partial T}{\partial t} + u_i T_{,i} = (\kappa T_{,i})_{,i} + \gamma \quad [3]$$

where  $u_i$ ,  $\sigma_{ij}$ ,  $T$ , and  $\gamma$  are the velocity, stress tensor, temperature, and heat-production rate, respectively,  $Ra$  is Rayleigh number, and  $\delta_{ij}$  is a Kronecker delta function. Repeated indexes denote summation, and  $u_{i,i}$  represents partial derivative of variable  $u$  with respect to coordinate  $x_i$ . These equations were obtained by using the following characteristic scales: length  $D$ , time  $D^2/\kappa$ ; and temperature  $\Delta T$ , where  $D$  is often the thickness of the mantle or a fluid layer,  $\kappa$  is thermal diffusivity, and  $\Delta T$  is the temperature difference across the fluid layer (*see* Chapters 7.02 and 7.04 for discussion on nondimensionalization). The stress tensor  $\sigma_{ij}$  can be related to strain rate  $\dot{\varepsilon}_{ij}$  via the following constitutive equation:

$$\sigma_{ij} = -P\delta_{ij} + 2\eta\dot{\varepsilon}_{ij} = -P\delta_{ij} + \eta(u_{i,j} + u_{j,i}) \quad [4]$$

where  $P$  is the dynamic pressure and  $\eta$  is the viscosity.

Substituting eqns [4] into [2] reveals three primary unknown variables: pressure, velocity, and temperature. The three governing eqns [1]–[3] are sufficient to solve for these three unknowns, together with adequate boundary and initial conditions. Initial conditions are only needed for temperature due to the first-order derivative with respect to time in the

energy equation. Boundary conditions are in general a combination of prescribed stress and velocity for the momentum equation, and of prescribed heat flux and temperature for the energy equation. The initial and boundary conditions can be expressed as

$$T(r_i, t = 0) = T_{\text{init}}(r_i) \quad [5]$$

$$u_i = g_i \text{ on } \Gamma_{g_i}, \quad \sigma_{ij}n_j = b_i \text{ on } \Gamma_{b_i} \quad [6]$$

$$T = T_{\text{bd}} \text{ on } \Gamma_{T_{\text{bd}}}, \quad (T_{,i})_n = q \text{ on } \Gamma_q \quad [7]$$

where  $\Gamma_{g_i}$  and  $\Gamma_{b_i}$  are the boundaries where  $i$ th components of velocity and forces are specified to be  $g_i$  and  $b_i$ , respectively,  $n_j$  is the normal vector of boundary  $\Gamma_{b_i}$ , and  $\Gamma_{T_{\text{bd}}}$  and  $\Gamma_q$  are the boundaries where temperature and heat flux are prescribed to be  $T_{\text{bd}}$  and  $q$ , respectively.

Often free-slip (i.e., zero tangential stresses and zero normal velocities) and isothermal conditions are applied to the surface and bottom boundaries in studies of mantle dynamics, although in some studies surface velocities may be given in consistent with surface plate motions (e.g., Bunge *et al.*, 1998). When steady-state or statistically steady-state solutions are to be sought, as they often are in mantle dynamics, the choice of initial condition can be rather arbitrary and it does not significantly affect final results in a statistical sense.

Although full time-dependent dynamics of thermal convection involves all three governing equations, an important subset of mantle dynamics problems, often termed as instantaneous Stokes flow problem, only require solutions of eqns [1] and [2]. For Stokes flow problem, one may consider the dynamic effects of a given buoyancy field (e.g., one derived from seismic structure) or prescribed surface plate motion on gravity anomalies, deformation rate, and stress at the surface and the interior of the mantle (Hager and O'Connell, 1981; Hager and Richards, 1989, also *see* Chapters 7.02 and 7.04).

These governing equations generally require numerical solution procedures for three reasons. (1) The advection of temperature in eqn [3],  $u_i T_{,i}$ , represents a nonlinear coupling between velocity and temperature. (2) The constitutive law or eqn [4] is often nonlinear in that stress and strain rate follow a power-law relation; that is, the viscosity  $\eta$  in eqn [4] can only be considered as effective viscosity that depends on stress or strain rate. (3) Even for the Stokes flow problem with a linear rheology, spatial variability in viscosity can make any analytic solution method difficult and impractical.

Irrespective of numerical methods used for the treatment of the individual governing equations, it is usual to solve the coupled system explicitly in time as follows: (1) At a given time step, solve eqns [1] and [2] (i.e., the instantaneous Stokes flow problem) for flow velocity for given buoyancy or temperature. (2) Update the temperature to next time step from eqn [3], using the new velocity field. (3) Continue this process of time stepping by going back to step (1).

### 7.05.3 Finite-Difference, Finite-Volume, and Spectral Methods

In this section, we will briefly discuss how finite-difference (FD), finite-volume (FV), and spectral methods are used in studies of mantle convection. These methods have a long history in modeling mantle convection (e.g., Machetel *et al.*, 1986; Gable *et al.*, 1991), and remain important in the field (e.g., Tackley, 2000; Kageyama and Sato, 2004; Stemmer *et al.*, 2006; Harder and Hansen, 2005).

#### 7.05.3.1 Finite Difference

FD methods have a much earlier historical beginning than FE, spectral, or FV methods because they are motivated intuitively by differential calculus and are based on local discretization of the derivative operators based on a Taylor series expansion with an assigned order of accuracy about a given point. The unknowns at each grid point depend on those of the neighboring points from the local Taylor expansion. For examples of FD implementation, the reader is urged to consult an excellent introductory book by Lynch (2005). Additional material of FORTRAN 95 listings of library subprograms using FD methods can be found in Griffiths and Smith (2006). Hence FD formulations are easy to grasp and to program and they have been the leading tool in numerical computations since the 1950s, as evidenced by the pioneering codes written for meteorology and applied weapons research (e.g., Richtmeyer and Morton, 1967). All of the initial codes in mantle convection were written with the FD formulation (Torrance and Turcotte, 1971; Turcotte *et al.*, 1973; McKenzie *et al.*, 1974; Parmentier *et al.*, 1975; Jarvis and McKenzie, 1980). The initial numerical techniques in solving mantle convection in the nonlinear regime were based on second-order FD methods (Torrance and Turcotte, 1971; McKenzie *et al.*, 1974). In the early 1980s, splines with a fourth-

order accuracy were used to solve two-dimensional (2-D) problems with variable viscosity (Christensen, 1984). Malevsky (1996) developed a 3-D mantle convection code based on 3-D splines, which allowed one to reach very high Rayleigh numbers, like  $10^8$  (Malevsky and Yuen, 1993). Recently, Kageyama and Sato (2004) have developed a 3-D FD technique, using a baseball-like topological configuration called the ‘yin–yang’ grid, for solving the 3-D spherical convection problem.

#### 7.05.3.1.1 FD implementation of the governing equations

For 2-D mantle convection within the Boussinesq approximation and isoviscous flow in FD methods, a commonly used formulation employs stream-function  $\Psi$  and vorticity  $\omega$  to eliminate the pressure and velocities, and the governing equations are written in terms of stream function  $\Psi$ , vorticity  $\omega$ , and temperature  $T$  (e.g., McKenzie *et al.*, 1974). They are written in time-dependent form as (also see eqns [1–3])

$$\nabla^2 \Psi = -\omega \quad [8]$$

$$\nabla^2 \omega = Ra \frac{\partial T}{\partial x} \quad [9]$$

$$\frac{\partial T}{\partial t} = \nabla^2 T - \left( \frac{\partial \Psi}{\partial x} \frac{\partial T}{\partial z} - \frac{\partial \Psi}{\partial z} \frac{\partial T}{\partial x} \right) + \gamma \quad [10]$$

where the velocity vector is defined as

$$\mathbf{v} = (v_x, v_z) = \left( \frac{\partial \Psi}{\partial z}, -\frac{\partial \Psi}{\partial x} \right) \quad [11]$$

which automatically satisfies the continuity, and  $\omega$  is the only component left of the vorticity vector  $\nabla \times \bar{v}$ ,  $x$  and  $z$  are the horizontal and vertical coordinates, respectively, with  $z$  vector pointing upward, and  $t$  is the time. We note that eqns [8] and [9] are given by a set of coupled second-order partial differential equations. Alternatively, we could have combined them to form a single fourth-order partial differential equation in terms of  $\Psi$ , called the biharmonic equation, as developed in the numerical scheme of Christensen (1984) using bicubic splines and also by Schott and Schmelting (1998) using FDs. We note that solving the biharmonic solution by FDs takes more time than solving two coupled Laplacian equations. We have restricted ourselves here to constant viscosity for pedagogical purposes. Examples of variable-viscosity convection equations

can be found in Christensen and Yuen (1984) and Schubert *et al.* (2000).

Zero tangential stress and impermeable boundary conditions can be expressed as

$$\omega|_{\Gamma} = \Psi|_{\Gamma} = 0 \quad [12]$$

Other boundary conditions are similar to those discussed in Section 7.05.2.

In 2-D mantle convection problems, one can also utilize the so-called primitive variables (i.e., velocity and dynamical pressure) formulation by solving the coupled equations of mass and momentum conservations at each time step. This procedure may involve more numerical care and computational time because of more unknowns. The examples can be found in Auth and Harder (1999) and Gerya and Yuen (2003, 2007).

For 3-D mantle convection, we can similarly employ the poloidal potential  $\Phi$  and a vorticity-like scalar function  $\Omega$  (Busse, 1989; Travis *et al.*, 1990). It is to be noted that this potential  $\Phi$  is not the same as the stream function  $\Psi$  in 2-D (*see* Chapter 7.04). From the general representation of an arbitrary solenoidal vector field (Busse, 1989), we can write a 3-D velocity vector as

$$\mathbf{v} = \nabla \times \nabla \times (\mathbf{e}_z \Phi) + \nabla \times (\mathbf{e}_z \Theta) \quad [13]$$

where  $\mathbf{e}_z$  is the unit vector in the vertical  $z$ -direction pointing upward.  $\Theta$  is the toroidal potential and is present in problems with lateral variations of viscosity (Zhang and Christensen, 1993; Gable *et al.*, 1991). Thus, for constant viscosity,  $\Theta$  is a constant and the velocity vector  $\mathbf{v} = (u, v, w)$  involves higher-order derivatives of  $\Phi$  in this formulation:

$$u = \frac{\partial^2 \Phi}{\partial y \partial z}, \quad v = \frac{\partial^2 \Phi}{\partial x \partial z}, \quad w = -\left(\frac{\partial^2 \Phi}{\partial x^2} + \frac{\partial^2 \Phi}{\partial y^2}\right) \quad [14]$$

The 3-D momentum equation for constant properties can be written as a system of coupled Poisson equations in 3-D:

$$\nabla^2 \Phi = \Omega \quad [15]$$

$$\nabla^2 \Omega = RaT \quad [16]$$

with the energy equation as

$$\frac{\partial T}{\partial t} = \nabla^2 T - \mathbf{v} \cdot \nabla T + \gamma \quad [17]$$

where all differential operators are 3-D in character, and  $\Omega$  is a scalar function playing a role analogous to the vorticity in the 2-D formulation.

We note that in FD and FV methods the primitive variables are now dominant in terms of popularity in 3-D mantle convection with variable viscosity (Tackley, 1994; Albers, 2000; Ogawa *et al.*, 1991; Trompert and Hansen, 1996).

### 7.05.3.1.2 Approximations of spatial derivatives and solution approaches

In FD methods, spatial derivations in the above equations need to be approximated by values at grid points. There are many algorithms for generating the formulas in the FD approximation of spatial differential operators (e.g., Kowalik and Murty, 1993; Lynch, 2005). The most common algorithm is to use a Taylor expansion. For example, a second-order differential operator (for simplicity, consider the spatial derivative in the  $x$ -direction) can be expressed as

$$\frac{d^2 f(x)}{dx^2} = [f(x_1) + f(x_3) - 2f(x_2)]/(\Delta x)^2 \quad [18]$$

where  $x_k$  is a grid point while the derivative is computed at a point  $x$  which is not necessarily a grid point (**Figure 1(a)**). This approximation is second-order accurate. We will use a recursive algorithm for generating the weights in the FD approximation with high-order accuracy. We will, for simplicity, consider the spatial derivative in the  $x$ -direction. The  $n$ th-order differential operator can be approximated by a FD operator as

$$\frac{d^n f(x)}{dx^n} = \sum_{k=1}^j W_{n,j,k} f(x_k) \quad [19]$$

where  $W_{n,j,k}$  are the weights to be applied at grid point  $x_k$  in order to calculate the  $n$ th order derivative at the point  $x$ . The stencil is  $j$  grid points wide. An ideal algorithm should accurately and efficiently produce weights for any order of approximation at arbitrarily distributed grid points. Such an algorithm has been developed and tested for simple differential operators by Fornberg (1990, 1995). The cost for generating each weight is just four operations and this can be done simply with a FORTRAN program given in Fornberg's book (Fornberg, 1995). The weights are collected in a 'differentiation matrix'. This results in calculating the derivatives of a vector, which is derived from a matrix–vector multiplicative operation. This algorithm can be easily generalized for determining the spatial derivatives for higher-dimensional operators.

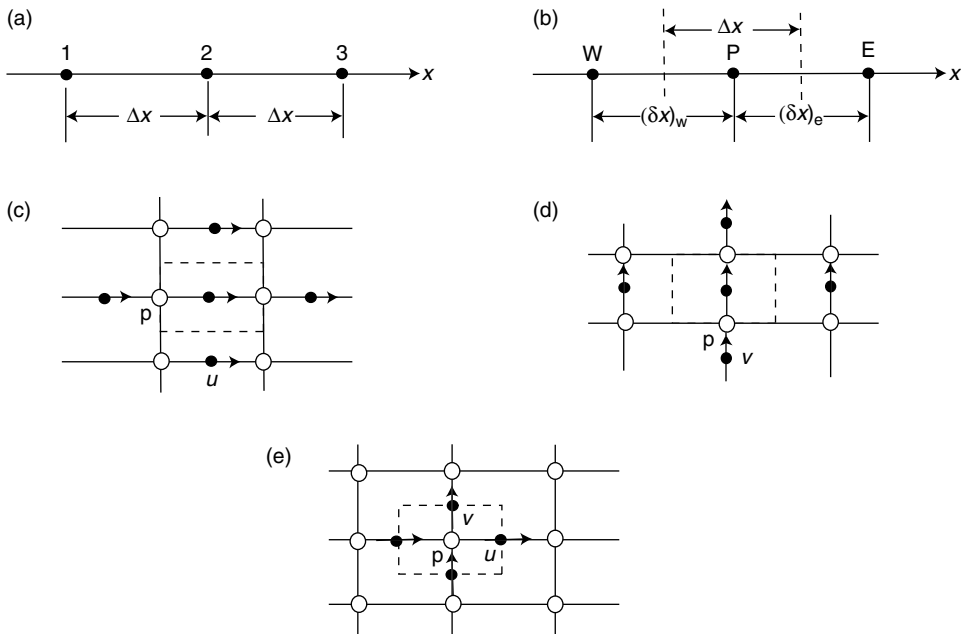


**Figure 1** A simple three-point one-dimensional (1-D) finite-difference stencil (a), a 1-D finite-volume control-cell (b), a staggered 2-D grid for velocity–pressure for horizontal (c) and vertical (d) components of the momentum equation and for the continuity equation (e).

In general, a  $p$ th-order FD method converges as  $O(k - p)$  for  $k$  grid points. However, variable coefficients and nonlinearities, such as the heat advection term, greatly complicate the convergence. The reader can find a more detailed discussion of the issues related to high-order FD methods and spectral methods in Fornberg (1995). Mantle convection in both 2-D and 3-D configurations using this variable-grid, high-order FD method has been studied by Larsen *et al.* (1995).

Using the stream-function vorticity formulation for 2-D and the scalar potential approach for 3-D, we can see that we have a large system of algebraic equations to solve at each time step. The partial differential equations posed by eqns [8] and [9] for 2-D and eqns [15] and [16] in 3-D represent one of the difficult aspects in mantle convection problems because of its elliptic nature. The linear algebra arising from this elliptic problem for large systems with varying size of matrix elements due to variable viscosity makes it very difficult to solve accurately. They can be written down symbolically as a large-scale matrix algebra problem,

$$Au = f \quad [20]$$

where  $A$  is a matrix operator involving the second-order spatial derivatives and the associated boundary

conditions for the stream function and vorticity,  $u$  is the solution vector over the set of 2-D grid points for  $(\Phi, \Omega)$ , and  $f$  is a vector representing the right-hand side of the system from eqns [8] and [9], namely  $\Omega$  and  $\partial T / \partial x$  values at 2-D grid points from the previous time step.

The matrix equation from 2-D mantle convection problems with variable viscosity can be solved effectively and very accurately with the direct method, such as the Cholesky decomposition, with current computational memory architecture. A high-resolution 2-D problem with around  $700 \times 700$  grid points and billions of tracers (Rudolf *et al.*, 2004) can be tackled on today's shared-memory machines with 1–2 TB of RAM memory, such as the S.G.I. Altix at National Center for Supercomputing Applications (NCSA) or the IBM Power-5 series in National Center for Atmospheric Research (NCAR). This tact of using shared-memory architecture has been employed by Gerya *et al.* (2006) to solve high-resolution 2-D convection problems with strongly variable viscosity. The presence of variable viscosity would make the matrix  $A$  very singular because of the disparity of values to the matrix elements. The adverse condition of the matrix is further aggravated by the presence of non-Newtonian rheology, which makes the matrix  $A$  nonlinear, thus making it

necessary to use iterative method for solving the matrix equation. Multigrid iterative method (e.g., Hackbusch, 1985; Press *et al.*, 1992; Trottenberg *et al.*, 2001; Yavneh, 2006) is a well-proven way of solving the elliptic problem with strong nonlinearities. Davies (1995) solved variable-viscosity convection problem in 2-D with the FD-based multigrid technique.

For 3-D mantle convection problems, one must still employ the iterative method because of memory requirements associated with a FD grid configuration with over a million unknowns. The multigrid iterative method used for an FD grid has been used by Parmentier and Sotin (2000) for solving 3-D high Rayleigh number mantle convection. We note that for variable-viscosity convection in 3-D one must use the pressure–velocity formulation cast in FDs (e.g., Peyret and Taylor, 1983) for the momentum equation. The resulting FD equations can be solved with the multigrid method. In this connection higher-order FD method (Fornberg, 1995) with variable grid points together with the multigrid technique may bring about a renaissance to the FD method because of its favorable posture in terms of memory requirements over FEs.

Another source of numerical difficulties in the mantle convection is due to the temperature advection term,  $\mathbf{v} \cdot \nabla T$ . It is well known from linear analysis that numerical oscillations result, if simple FD schemes are used to calculate the spatial derivative due to the interaction between velocity and the FD approximations of  $\nabla T$ . Excellent discussions of this problem involving numerical dispersion can be found in Kowalik and Murty (1993). Different numerical approximations have been proposed to treat the advection term in the FD: the first is by Spalding (1972), which involves a weighted upwind scheme and is first-order accurate, which has been employed in the early FD codes of mantle convection (Turcotte *et al.*, 1973). A more popular and effective method is an iterated upwind correction scheme that is correct to second order and was proposed by Smolarkiewicz (1983, 1984). This is a scheme based on the positively definite character of the advection term. The solutions, in general, do not change much after one to two correction steps and it is easy to program for parallel computers. This scheme has been implemented by Parmentier and Sotin (2000) and by Tackley (2000) for mantle convection problems. Use of higher-order FD schemes (Fornberg, 1995) will also help to increase the accuracy of the advection of

temperature because this will lead closer to a pseudospectral quality. Other advection schemes include the semi-Lagrangian technique, which is based on tracer characteristics and have been used in mantle convection for the stream-function method (Malevsky and Yuen, 1991) and for primitive variables (Gerya and Yuen, 2003).

### 7.05.3.2 FV Method

A FV method is often used to solve differential equations (Patankar, 1980). FV methods share some common features with FE and FD methods. In FV methods, discretization of a differential equation results from integrating the equation over a control-volume or control-cell and approximating differential operators of reduced order at cell boundaries (Patankar, 1980). Patankar (1980) suggested that the FV formulation may be considered as a special case of the weighted residual method in FE in which the weighting function is uniformly one within an element and zero outside of the element. The FV method is also similar to FD method in that they both need to approximate differential operators using values at grid points.

We will use a simple example to illustrate the basic idea of the FV method (Patankar, 1980). Consider a 1-D heat conduction equation with heat source  $\gamma$ .

$$\frac{d}{dx} \left( k \frac{dT}{dx} \right) + \gamma = 0 \quad [21]$$

where  $k$  is the heat conductivity. This equation is integrated over a control-cell bounded by dashed lines in **Figure 1(b)**, and the resulting equation is

$$\left( k \frac{dT}{dx} \right)_e - \left( k \frac{dT}{dx} \right)_w + \int_w^e \gamma dx = 0 \quad [22]$$

where  $e$  and  $w$  represent the two ends of the control-cell (**Figure 1(b)**). Introducing approximations for the flux at each end and the source term in eqn [22] leads to

$$\frac{k_e(T_E - T_P)}{(\delta x)_e} - \frac{k_w(T_P - T_W)}{(\delta x)_w} + \bar{\gamma} \Delta x = 0 \quad [23]$$

where  $k_e$  and  $k_w$  are the heat conductivity at cell boundaries,  $T_E$ ,  $T_P$ , and  $T_W$  are temperatures at nodal points,  $\bar{\gamma}$  is the averaged source in the control-cell, and  $\Delta x = [(\delta x)_e + (\delta x)_w]/2$  is the size of the control-cell (**Figure 1(b)**). The eqn [23] is a discrete equation with nodal temperatures as

unknown for the given control-cell. Applying this procedure to all control-cells leads to a system of equations with unknown temperatures at all grid points, similar to eqn [20] from a FD method.

FV methods have also been used extensively in modeling mantle convection, possibly starting with Ogawa *et al.* (1991). Tackley (1994) implemented an FV method coupled with a multigrid solver for 2-D/3-D Cartesian models. Ratcliff *et al.* (1996) developed a 3-D spherical-shell model of mantle convection using an FV method. Harder and Hansen (2005) and Stemmer *et al.* (2006) also developed FV mantle convection codes for spherical-shell geometries using a cubed sphere grid. All these mantle convection studies used second-order accurate FV methods, although higher-order formulas can be formulated.

To solve fluid flow problems that are governed by the continuity and momentum equations, such as those in mantle convection, it is often convenient to use the pressure–velocity formulation, similar to FE method. Also, a staggered grid is often used in which pressures and velocities are defined at different locations of a control-cell (Patankar, 1980; Tackley, 1994) (**Figures 1(c)–1(e)**). Such a staggered grid helps remove checkerboard pressure solutions. In the staggered grid, control-cells for the momentum equation are different from those for the continuity equation. For example, for the continuity equation, a pressure node is at the center of a control-cell, while velocities are defined at the cell boundaries such that each velocity component is perpendicular to the corresponding cell boundary (**Figure 1(e)**). For the momentum equation, the velocities are at the center of a cell, while the pressures are defined at cell boundaries (**Figures 1(c)** and **1(d)**).

For a given pressure field, applying the FV procedure leads to discrete equations for velocities. However, solutions to the velocity equations are only accurate if the pressure field is accurate. The continuity equation is used to correct the pressure field. This iterative procedure between the velocity and pressure is implemented efficiently in a SIMPLER algorithm (Patankar, 1980) that is used in the FV convection codes (Tackley, 1993, 1994; Stemmer *et al.*, 2006). A variety of methods can be used to solve the discrete equations of velocities and pressure, similar to that in FD method. They may include successive over-relaxation and Gauss–Seidel iteration (Harder and Hansen, 2005; Stemmer *et al.*, 2006), or a multigrid method (Tackley, 1994), or the alternating-direction implicit (i.e., ADI) method (Monnereau and Yuen, 2002).

Like in FE and FD methods, the FV method also requires special treatment of advection term  $\mathbf{v} \cdot \nabla T$  in the energy equation. Either upwind scheme or an iterative correction scheme such as that proposed by Smolarkiewicz (1983, 1984) in Section 7.05.3.1 on FD can be used in the FV method to treat the advection term.

### 7.05.3.3 Spectral Methods

The spectral method is a classical method, which is motivated by its analytical popularity and inherent accuracy. It is based on the concept of orthogonal eigenfunction expansion based on the differential operators associated with the Laplace equation and works on orthogonal curvilinear coordinate systems. For mantle convection problems this means that we can express the horizontal dependence by using Fourier expansion for Cartesian geometry and spherical harmonics for the 3-D spherical shell. Symbolically we can write down this expansion as

$$F(x_1, x_2, x_3) = \sum_{ijk} a_{ijk} f(x_3) g(x_1) h(x_2) \quad [24]$$

where  $F$  is the field variable being expanded,  $a_{ijk}$  is the spectral coefficient,  $x_1$  and  $x_2$  are the horizontal coordinates,  $x_3$  is the vertical or radial coordinate,  $g$  and  $h$  are the eigenfunctions being employed, and  $f$  is a function describing the vertical or radial dependence. We note that  $f$  can be determined by solving a two-point boundary value, using propagator matrices, or an orthogonal function expansion, as in the case of Chebychev polynomials, or using the FD (e.g., Cserepes and Rabionowicz, 1985; Cserepes *et al.*, 1988; Gable *et al.*, 1991; Travis *et al.*, 1990; Machetel *et al.*, 1986; Glatzmaier, 1988).

Balachandar and Yuen (1994) developed a spectral-transform 3-D Cartesian code for mantle convection, based on expansion of Chebychev functions for solving the two-point boundary-value problem in the vertical direction and fast Fourier transforms along the two horizontal directions. This method has also been extended to variable-viscosity problems with the help of Krylov subspace iterative technique (Saad and Schultz, 1986) for solving iteratively the momentum equation. The first 3-D codes in spherical-shell convection were developed by Machetel *et al.* (1986) who used an FD scheme in the radial direction and spherical harmonic decomposition over the longitudinal and latitudinal directions and by Glatzmaier (1988) who employed Chebychev polynomials in solving

the radial direction and spherical harmonics for the spherical surface. The Chebychev polynomials allow for very high accuracy near the thermal boundary layers. They can also be expanded about internal boundary layers, such as the one at 670 km discontinuity. Zhang and Yuen (1995 and 1996a) have devised a 3-D code for spherical geometry based on higher-order FD method (Fornberg, 1995) and spectral expansion in the field variables in spherical harmonics along the circumferential directions. They also developed an iterative technique for the momentum equation to solve for variable viscosity with a lateral viscosity contrast up to 200 (Zhang and Yuen, 1996b) in compressible convection. It is important to check also the spectra of the viscosity decay with the degree of the spherical harmonics (Zhang and Yuen, 1996a) in order to ascertain whether Gibbs phenomenon is present.

Spectral methods are very accurate, much more so than FEs and FDs for the same computational efforts, and their efficacy in terms of convergence can be assessed by examining the rate of decay of the energy in the spectrum with increasing number of terms in the spectral expansion in eqn [24] (Peyret and Taylor, 1983). Spectral methods also have a couple of other distinct advantages. First, they are very easy to implement, because they reduce the problems to either an algebraic set or simple weakly coupled ordinary differential equations, as discussed earlier. Second, using fast transform algorithms such as fast Fourier transform, spectral methods can be very efficient and fast on a single-processor computer.

However, spectral methods only work well for constant material properties or depth-dependent properties in simple geometries (Balachandar and Yuen, 1994). Furthermore, spectral techniques do not go as far in terms of viscosity contrasts (less than a factor of 200) for variable-viscosity convection (Balachandar *et al.*, 1995, Zhang and Yuen, 1996b). We note, however, that Schmalholz *et al.* (2001) showed that in a folding problem their spectral method could go up to a viscosity contrast of around  $10^4$ . Perhaps a better choice of a preconditioner in the solution of the momentum equation in the spectral expansion of a variable-viscosity problem will enable a larger viscosity contrast than  $10^4$ . This issue is still open and remains a viable research topic. Spectral methods are also difficult to be used efficiently on parallel computers because of the global basis functions used in these methods. At present, spectral methods, although elegant mathematically, are not as effective as other numerical methods for solving

realistic mantle convection problems. Spectral methods still remain the main driver for geodynamo problems (e.g., Glatzmaier and Roberts, 1996; Kuang and Bloxham, 1999) because of the exclusive choice of constant material properties in solving the set of magneto-hydrodynamic equations. Lastly, we wish to mention briefly a related spectral method called the spectral-element method (Maday and Patera, 1989), which is now being used in geophysics in seismic-wave propagation (Komatitsch and Tromp, 1999). This approach may hold some promise for variable-viscosity mantle convection.

### 7.05.4 An FE Method

FE methods are effective in solving differential equations with complicated geometry and material properties. FE methods have been widely used in the studies of mantle dynamics (Christensen, 1984; Baumgardner, 1985; King *et al.*, 1990; van den Berg *et al.*, 1993; Moresi and Gurnis, 1996; Bunge *et al.*, 1997; Zhong *et al.*, 2000). This section will go through some of the basic steps in using FE methods in solving governing equations for thermal convection.

The FE formulation for Stokes flow that is described by eqns [1] and [2] is independent from that for the energy equation. Hughes (2000) gave detailed description on a Galerkin weak-form FE formulation for the Stokes flow. Brooks (1981) developed a streamline upwind Petrov–Galerkin formulation (SUPG) for the energy equation involving advection and diffusion. These two formulations remain popular for solving these types of problems (Hughes, 2000) and are employed in mantle convection codes ConMan (King *et al.*, 1990) and Citcom/CitcomS (Moresi and Gurnis, 1996; Zhong *et al.*, 2000). The descriptions presented here are tailored from Brooks (1981), Hughes (2000), and Ramage and Wathen (1994) specifically for thermal convection in an incompressible medium, and they are also closely related to codes ConMan and Citcom.

#### 7.05.4.1 Stokes Flow: A Weak Formulation, Its FE Implementation, and Solution

##### 7.05.4.1.1 A weak formulation

The Galerkin weak formulation for the Stokes flow can be stated as follows: find the flow velocity  $u_j = v_i + g_i$  and pressure  $P$ , where  $g_i$  is the prescribed boundary velocity from eqn [6] and  $v_i \in \mathbf{V}$ , and  $P \in \mathbf{P}$ , where  $\mathbf{V}$  is a set of functions in which each function,

$w_i$ , is equal to zero on  $\Gamma_{\text{g}}$ , and  $\mathbf{P}$  is a set of functions  $q$ , such that for all  $w_i \in \mathbf{V}$  and  $q \in \mathbf{P}$

$$\int_{\Omega} w_{i,j} \sigma_{ij} d\Omega - \int_{\Omega} q u_{i,i} d\Omega = \int_{\Omega} w_i f_i d\Omega + \sum_{i=1}^{n_{\text{sd}}} \int_{\Gamma_{b_i}} w_i b_i d\Gamma \quad [25]$$

$w_i$  and  $q$  are also called weighting functions. Equation [25] is equivalent to eqns [1] and [2] and boundary conditions equation [6], provided that  $f_i = RaT\delta_{iz}$  (Hughes, 2000). Equation [25] can be written as

$$\int_{\Omega} w_{i,j} c_{ijkl} v_{k,l} d\Omega - \int_{\Omega} q v_{i,i} d\Omega - \int_{\Omega} w_i P d\Omega = \int_{\Omega} w_i f_i d\Omega + \sum_{i=1}^{n_{\text{sd}}} \int_{\Gamma_{b_i}} w_i b_i d\Gamma - \int_{\Omega} w_{i,j} c_{ijkl} g_{k,l} d\Omega \quad [26]$$

where

$$c_{ijkl} = \eta(\delta_{ik}\delta_{jl} + \delta_{il}\delta_{jk}) \quad [27]$$

is derived from constitutive eqn [4]. It is often convenient to rewrite

$$w_{i,j} c_{ijkl} v_{k,l} = \varepsilon(\mathbf{w})^T D \varepsilon(\mathbf{v}) \quad [28]$$

where for 2-D plane strain problems,

$$\varepsilon(\mathbf{v}) = \begin{Bmatrix} v_{1,1} \\ v_{2,2} \\ v_{1,2} + v_{2,1} \end{Bmatrix}, \quad D = \begin{bmatrix} 2\eta & 0 & 0 \\ 0 & 2\eta & 0 \\ 0 & 0 & \eta \end{bmatrix} \quad [29]$$

(note here the change in the definition of the off-diagonal components of the strain-rate tensor). It is straightforward to write the expressions for other coordinate systems including 3-D Cartesian, axisymmetric (Hughes, 2000), or spherical geometry (Zhong et al., 2000).

Suppose that we discretize the solution domain  $\Omega$  using a set of grid points (**Figure 2**) so that the velocity and pressure fields and their weighting functions can be expressed anywhere in the domain in terms of their values at the grid (nodal) points and the so-called ‘shape functions’ which interpolate the grid points:

$$\begin{aligned} \mathbf{v} &= v_i \mathbf{e}_i = \sum_{A \in \Omega^v - \Gamma_{\text{g}}^v} N_A v_{iA} \mathbf{e}_i, \\ \mathbf{w} &= w_i \mathbf{e}_i = \sum_{A \in \Omega^v - \Gamma_{\text{g}}^v} N_A w_{iA} \mathbf{e}_i, \\ \mathbf{g} &= \sum_{A \in \Gamma_{\text{g}}^v} N_A g_{iA} \mathbf{e}_i \end{aligned} \quad [30]$$

$$P = \sum_{B \in \Omega^p} M_B P_B, \quad q = \sum_{B \in \Omega^p} M_B q_B \quad [31]$$

where  $N_A$  is the shape functions for velocity at node A,  $M_B$  is the shape functions for pressure at node B,

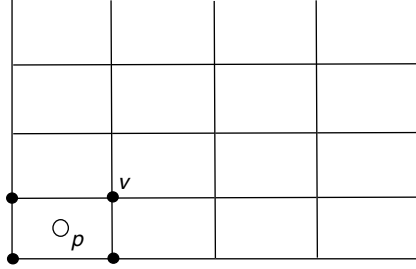


**Figure 2** Finite-element discretization and grid in 2-D. For a four-node bilinear element, the pressure is defined at the center of the element, while velocities are defined at the four corners.

$\Omega^v$  is the set of velocity nodes,  $\Omega^p$  is the set of pressure nodes, and  $\Gamma_{\text{g}}^v$  is the set of velocity nodes along boundary  $\Gamma_{\text{g}}$ . Note that the velocity shape functions and velocity nodes can be (and usually are) different from those for pressure (**Figure 2**).

Substituting eqns [30] into [28] leads to the following equation:

$$\begin{aligned} \varepsilon(\mathbf{w})^T D \varepsilon(\mathbf{v}) &= \varepsilon \left( \sum_{A \in \Omega^v - \Gamma_{\text{g}}^v} N_A w_{iA} \mathbf{e}_i \right)^T D \varepsilon \left( \sum_{B \in \Omega^v - \Gamma_{\text{g}}^v} N_B v_{jB} \mathbf{e}_j \right) \\ &= \left[ \sum_{A \in \Omega^v - \Gamma_{\text{g}}^v} \varepsilon(N_A \mathbf{e}_i)^T w_{iA} \right] D \left[ \sum_{B \in \Omega^v - \Gamma_{\text{g}}^v} \varepsilon(N_B \mathbf{e}_j) v_{jB} \right] \\ &= \sum_{A \in \Omega^v - \Gamma_{\text{g}}^v} w_{iA} \left[ \sum_{B \in \Omega^v - \Gamma_{\text{g}}^v} \mathbf{e}_i^T B_A^T D B_B \mathbf{e}_j v_{jB} \right] \end{aligned} \quad [32]$$

where for 2-D plane strain problems

$$B_A = \begin{bmatrix} N_{A,1} & 0 \\ 0 & N_{A,2} \\ N_{A,2} & N_{A,1} \end{bmatrix} \quad [33]$$

Substituting eqns [30] and [31] into [26] leads to the following equation:

$$\begin{aligned} \sum_{A \in \Omega^v - \Gamma_{\text{g}}^v} w_{iA} \left[ \sum_{B \in \Omega^v - \Gamma_{\text{g}}^v} \left( \mathbf{e}_i^T \int_{\Omega} B_A^T D B_B d\Omega \mathbf{e}_j v_{jB} \right) \right. \\ \left. - \sum_{B \in \Omega^p} \left( \mathbf{e}_i^T \int_{\Omega} N_{A,i} M_B d\Omega P_B \right) \right] \\ - \sum_{A \in \Omega^p} \left[ q_A \sum_{B \in \Omega^v - \Gamma_{\text{g}}^v} \left( \int_{\Omega} M_A N_{B,j} d\Omega \mathbf{e}_j g_{jB} \right) \right] \\ = \sum_{A \in \Omega^v - \Gamma_{\text{g}}^v} w_{iA} \left[ \int_{\Omega} N_A \mathbf{e}_i f_i d\Omega + \sum_{i=1}^{n_{\text{sd}}} \int_{\Gamma_{b_i}} N_A \mathbf{e}_i b_i d\Gamma \right. \\ \left. - \sum_{B \in \Gamma_{\text{g}}^v} \left( \mathbf{e}_i^T \int_{\Omega} B_A^T D B_B d\Omega \mathbf{e}_j g_{jB} \right) \right] \end{aligned} \quad [34]$$

Because eqn [34] holds for any weighting functions  $w_{iA}$  and  $q_A$ , it implies the following two equations:

$$\begin{aligned} & \sum_{B \in \Omega^v - \Gamma_{\mathcal{S}}^v} \left( \mathbf{e}_i^T \int_{\Omega} B_A^T D B_B d\Omega \mathbf{e}_j v_{jB} \right) \\ & - \sum_{B \in \Omega^v} \left( \mathbf{e}_i^T \int_{\Omega} N_{A,i} M_B d\Omega P_B \right) \\ & = \int_{\Omega} N_A \mathbf{e}_i f_i d\Omega + \sum_{i=1}^{n_{sd}} \int_{\Gamma_{B_i}} N_A \mathbf{e}_i b_i d\Gamma \\ & - \sum_{B \in \Gamma_{\mathcal{S}}^v} \left( \mathbf{e}_i^T \int_{\Omega} B_A^T D B_B d\Omega \mathbf{e}_j g_{jB} \right) \quad [35] \end{aligned}$$

$$\sum_{B \in \Omega^v - \Gamma_{\mathcal{S}}^v} \left( \int_{\Omega} M_A N_{B,j} d\Omega \mathbf{e}_j v_{jB} \right) = 0 \quad [36]$$

Combining eqns [35] and [36] into a matrix form leads to

$$\begin{bmatrix} K & G \\ G^T & 0 \end{bmatrix} \begin{Bmatrix} V \\ P \end{Bmatrix} = \begin{Bmatrix} F \\ 0 \end{Bmatrix} \quad [37]$$

where the vector  $V$  contains the velocity at all the nodal points, the vector  $P$  is the pressure at all the pressure nodes, the vector  $F$  is the total force term resulting from the three terms on the right-hand side of eqn [35], the matrices  $K$ ,  $G$ , and  $G^T$  are the stiffness matrix, discrete gradient operator, and discrete divergence operator, respectively, which are derived from the first and second terms of eqns [35] and [36], respectively. Specifically, the stiffness matrix is given by

$$K_{lm} = \mathbf{e}_i^T \int_{\Omega} B_A^T D B_B d\Omega \mathbf{e}_j \quad [38]$$

where subscripts A and B are the global velocity node numbers as in eqn [30],  $i$  and  $j$  are the degree of freedom numbers ranging from 1 to  $n_{sd}$ , and  $l$  and  $m$  are the global equation numbers for the velocity ranging from 1 to  $n_v n_{sd}$  where  $n_v$  is the number of velocity nodes.

#### 7.05.4.1.2 An FE implementation

We now present an FE implementation of the Galerkin weak formulation for the Stokes flow and the resulting expressions of different terms in [37]. A key point of the FE approach is that all of the equations to be solved are written in the form

of integrals over the solution domain and can, therefore, without approximation, be written as a sum of integrals over convenient subdomains, and the matrix eqn [37] may be decomposed into overlapping sums of contributions from these domains.

Let us first introduce the elements and shape functions. A key feature of the standard FE method is that a local basis function or shape function is used such that the value of a variable within an element depends only on that at nodal points of the element. The shape functions are generally chosen such that they have the value of unity on their parent node and zero at all other nodes and zero outside the boundary of the element. Unless there is a special, known form to the solution, it is usual to choose simple polynomial shape functions and form their products for additional dimensions. In addition, this interpolating requirement constrains the patterns of nodes in an element and which elements can be placed adjacent to each other. Bathe (1996) gives an excellent overview of the issues. (As usual, there are some useful exceptions to this rule, one being the element-free Galerkin method where smooth, overlapping interpolating kernels are used. This does mean, however, that the global problem cannot be trivially decomposed into local elements.) Zienkiewicz *et al.* (2005) is also an excellent source of reference for these topics.

For simplicity, we consider a 2-D domain with quadrilateral elements. We employ mixed elements in which there are four velocity nodes per element each of which occupies a corner of the element, while the only pressure node is at the center of the element (**Figure 2**). For these quadrilateral elements, the velocity interpolation in each element uses bilinear shape functions, while the pressure is constant for each element.

As a general remark on FE modeling of deformation/flow of incompressible media, it is important to keep interpolation functions (shape functions) for velocities at least 1 order higher than those for pressure, as we did for our quadrilateral elements (Hughes, 2000). Spurious flow solutions may arise sometimes even if this condition is satisfied. The best-known example is the ‘mesh locking’ that arises from linear triangle elements with constant pressure per element for which incompressibility (i.e., a fixed elemental area) constraint per element demands zero deformation/flow everywhere in the domain (Hughes, 2000).

For any given element  $e$ , velocity and pressure within this element can be expressed through the following interpolation:

$$\mathbf{v} = v_i \mathbf{e}_i = \sum_{a=1}^{n_{en}} N_a v_{ia} \mathbf{e}_i, \quad \mathbf{w} = w_i \mathbf{e}_i = \sum_{b=1}^{n_{en}} N_b w_{ib} \mathbf{e}_i, \\ \mathbf{g} = g_i \mathbf{e}_i = \sum_{a=1}^{n_{en}} N_a g_{ia} \mathbf{e}_i \quad [39]$$

$$P = \sum_{a=1}^{n_{ep}} M_a P_a, \quad q = \sum_{a=1}^{n_{ep}} M_a q_a \quad [40]$$

where  $n_{en}$  and  $n_{ep}$  are the numbers of velocity and pressure nodes per element, respectively, and  $n_{en}=4$  and  $n_{ep}=1$  for our quadrilateral elements. The shape function  $N_a$  for  $a=1, \dots, n_{en}$  depends on coordinates, and  $N_a$  is 1 at node  $a$  and linearly decreases to zero at other nodes of the element. The locality of the shape functions greatly simplifies implementation and computational aspects of the Galerkin weak formulation. For example, the integrals in eqns [35] and [36] may be decomposed into sum of integrals from each element and the matrix equation [37] may be decomposed into sums of elemental contributions. Specifically, we may now introduce elemental stiffness matrix, discrete gradient and divergence operators, and force term.

$$k^e = [k_{lm}^e], \quad g^e = [g_{ln}^e], \quad f^e = \{f_l^e\} \quad [41]$$

where  $1 \leq l, m \leq n_{en} n_{sd}$ ,  $1 \leq n \leq n_{ep}$  (note that for quadrilateral elements,  $n_{en}=4$ ,  $n_{ep}=1$ , and  $n_{sd}=2$ ),  $k^e$  is a square matrix of  $n_{en} n_{sd}$  by  $n_{en} n_{sd}$ , and  $g^e$  is a matrix of  $n_{en} n_{sd}$  by  $n_{ep}$ .

$$k_{lm}^e = \mathbf{e}_i^T \int_{\Omega^e} B_a^T D B_b d\Omega \mathbf{e}_j \quad [42]$$

where  $l=n_{sd}(a-1)+i$ ,  $m=n_{sd}(b-1)+j$ ,  $a, b=1, \dots, n_{en}$ , and  $i, j=1, \dots, n_{sd}$

$$g_{ln}^e = -\mathbf{e}_i \int_{\Omega^e} N_{a,i} M_n d\Omega \quad [43]$$

where  $n=1, \dots, n_{ep}$ , and the rest of the symbols have the same definitions as before:

$$f_l^e = \int_{\Omega^e} N_a f_i d\Omega + \int_{\Gamma_{b_i}^e} N_a b_i d\Gamma - \sum_{m=1}^{n_{sd} n_{en}} k_{lm}^e g_m^e \quad [44]$$

Determinations of these elemental matrices and force term require evaluations of integrals over each element with integrands that involve the shape functions and their derivatives. It is often convenient to

use isoparametric elements for which the coordinates and velocities in an element have the interpolation schemes (Hughes, 2000). For example, for 2-D quadrilateral elements that we discussed earlier, the velocity shape functions for node  $a$  of an element in a parent domain with coordinates  $\xi \in (-1, 1)$  and  $\eta \in (-1, 1)$  is given as

$$N_a(\xi, \eta) = 1/4(1 + \xi_a \xi)(1 + \eta_a \eta) \quad [45]$$

where  $(\xi_a, \eta_a)$  is  $(-1, -1)$ ,  $(1, -1)$ ,  $(1, 1)$ , and  $(-1, 1)$  for  $a = 1, 2, 3$ , and  $4$ , respectively. The pressure shape functions for  $M_a$  is 1, as there is only one pressure node per element. Although the integrations in [42]–[44] are in the physical domain (i.e.,  $x_1$  and  $x_2$  coordinates) rather than the parent domain, they can be expressed in the parent domain through coordinate transformation.

In practice, these element integrals are calculated numerically by some form of quadrature rule. In 2-D, Gaussian quadrature rules are optimal and are usually recommended; in 3-D, other rules may be more efficient but are not commonly used for reasons of programming simplicity (Hughes (2000) documents integration procedure in detail). There are a small number of cases where it may be worthwhile using a nonstandard procedure to integrate an element. The most common is where the constitutive parameters (i.e.,  $D$  in eqn [29]) change within the element; a higher-order quadrature scheme than the standard recommended one can give improved accuracy in computing  $k^e$ . When the constitutive parameters are strongly history dependent,  $D$  is known only at a number of Lagrangian sample points; if these are used directly to integrate  $k^e$ , the Lagrangian integration point methods such as MPM result (Sulsky *et al.*, 1994; Moresi *et al.*, 2003 for application in geodynamics).

With elemental  $k^e$ ,  $g^e$ , and  $f^e$  determined, it is straightforward to assemble them into global matrix eqn [37]. If an iterative solution method is used to solve [37], one may carry out calculations of the left-hand side of [37] element by element without assembling elemental matrices and force terms into the global matrix equation form [37].

The boundary conditions described in eqn [44] are simple to implement when the boundary is aligned with the coordinate system, and when the boundary condition is purely velocity or purely boundary tractions. The difficulty arises in the case of boundaries which are not aligned with the coordinate system and which specify a mixture of

boundary tractions and velocities. This form of boundary condition is common in engineering applications of FE method, designing mechanical components, for example, and in geodynamics it occurs when modeling arbitrarily oriented contact surfaces such as faults, or a spherical boundary in a Cartesian solution domain. Unless treated appropriately, this form of boundary condition leads to a constraint on a linear combination of the degrees of freedom at each constrained node. The solution is straightforward: instead of using the global coordinate system to form the matrix equation, we first transform to a local coordinate system which does conform to the boundary geometry (Desai and Abel, 1972).

Let  $R$  be a rotation matrix which transforms the global coordinate system XYZO to a local one X'Y'Z'O' aligned with the boundary at node  $n$ . The transformed stiffness matrix and force vector contributions for this node then become

$$K'_n = R_n^T K_n R_n \quad [46]$$

and

$$F'_n = R_n^T F_n \quad [47]$$

$R$  can be formulated for each node or it may be assembled for an element or for the global matrices but, other than the nodes where the ‘skew’ boundary conditions occur, the block entries are simply the identity matrix. It is possible to use this procedure at every node in a system with a natural coordinate system (e.g., the spherical domain) so that one can switch freely between a spherical description of forces and velocities where convenient, and an underlying Cartesian formulation of the constitutive relations. This method was used in modeling faults in Zhong *et al.* (1998).

#### 7.05.4.1.3 The Uzawa algorithm for the matrix equation

Similar to FD or FV methods, the FE discretization of the differential equations leads to a matrix equation such as [37]. The remaining question is to solve the matrix equation, which we now discuss in this section. We can use either direct or iterative methods to solve the matrix equation, depending on problems that we are interested, similar to what we discussed earlier for matrix equation [20] from FD method. Here we will focus on iterative solution methods, because they require significantly less memory and computation than direct solution approaches.

Iterative solution approaches are the only feasible and practical approaches for 3-D problems. Later we will briefly discuss a penalty formulation for the incompressible Stokes flow that requires a direct solution approach and is only effective for 2-D problems.

The system of equations as it stands is singular due to the block of zero entries in the diagonal, but it is symmetric, and the stiffness matrix  $K$  is symmetric positive definite and we can use this to our advantage in finding a solution strategy. An efficient method is the Uzawa algorithm which is implemented in Citcom code (Moresi and Solomatov, 1995). In the Uzawa algorithm, the matrix equation [37] is broken into two coupled systems of equations (Atanga and Silvester, 1992; Ramage and Wathen, 1994):

$$KV + GP = F \quad [48]$$

$$G^T V = 0 \quad [49]$$

Combining these two equations and eliminating  $V$  to form the Schur complement system for pressure (Hughes, 2000)

$$(G^T K^{-1} G)P = G^T K^{-1} F \quad [50]$$

Notice that matrix  $\hat{K} = G^T K^{-1} G$  is symmetric positive definite. Although in practice eqn [51] cannot be directly used to solve for  $P$  due to difficulties in obtaining  $K^{-1}$ , we may use it to build a pressure-correction approach by using a conjugate gradient algorithm which does not require construction of matrix  $\hat{K}$  (Ramage and Wathen, 1994). The procedure is presented and discussed in detail as follows.

With the conjugate gradient algorithm, for symmetric positive definite  $\hat{K}$ , the solution to a linear system of equations  $\hat{K}P = H$  can be obtained with the operations in the left column of **Figure 3** (Golub and van Loan, 1989, p. 523).

For equations [48] and [50] for both velocities and pressure, with initial guess pressure  $P_0 = 0$ , the initial velocity  $V_0$  can be obtained from

$$KV_0 = F, \quad \text{or} \quad V_0 = K^{-1} F \quad [51]$$

and the initial residual for pressure equation [50],  $r_0$ , and search direction,  $s_1$ , are  $r_0 = s_1 = H = G^T K^{-1} F = G^T V_0$  (see the left column of **Figure 3**). To determine the search step  $\alpha_k$  in the conjugate gradient algorithm, we need to compute the product of search direction  $s_k$  and  $\hat{K}$ ,  $s_k^T \hat{K} s_k$  (**Figure 3**). This product can be evaluated without explicitly constructing  $\hat{K}$  for the following reasons.

```

k=0; P0=0; r0=H
while |rk|>a given tolerance, ε
    k=k+1
    if k=1
        s1=r0
    else
        βk=rk-1Trk-1/rk-2Trk-2
        sk=rk-1+βksk-1
    end
    αk=rk-1Trk-1/skT^Ksk
    Pk=Pk-1+αksk
    rk=rk-1+αkKsk
end
P=Pk

```

```

k=0; P0=0
Solve KV0=F
r0=H=GTV0
while |rk|>a given tolerance, ε
    k=k+1
    if k=1
        s1=r0
    else
        βk=rk-1Trk-1/rk-2Trk-2
        sk=rk-1+βksk-1
    end
    Solve Kuk=Gsk
    αk=rk-1Trk-1/(Gsk)Tuk
    Pk=Pk-1+αksk
    Vk=Vk-1-αkuk
    rk=rk-1-αkGTuk
end
P=Pk, V=Vk

```

**Figure 3** The left column is the original conjugate gradient algorithm, and the right column is the Uzawa algorithm for solving eqns [48] and [49].

The product can be written as

$$s_k^T \hat{K} s_k = s_k^T G^T K^{-1} G s_k = (G s_k)^T K^{-1} G s_k \quad [52]$$

If we define  $u_k$  such that

$$K u_k = G s_k, \quad \text{or} \quad u_k = K^{-1} G s_k \quad [53]$$

then we have

$$s_k^T \hat{K} s_k = (G s_k)^T K^{-1} G s_k = (G s_k)^T u_k \quad [54]$$

This indicates that if we solve [53] for  $u_k$  with  $G s_k$  as the force term, the product  $s_k^T \hat{K} s_k$  can be obtained without actually forming  $\hat{K}$ . Similarly,  $\hat{K} s_k$  in updating the residual  $r_k$  (the left column of **Figure 3**) can be obtained without forming  $\hat{K}$ , because

$$\hat{K} s_k = G^T K^{-1} G s_k = G^T u_k$$

As the pressure  $P$  is updated via  $P_k = P_{k-1} + \alpha_k s_k$  from the conjugate gradient algorithm (**Figure 3**), the velocity field can also be updated accordingly via

$$V_k = V_{k-1} - \alpha_k u_k \quad [55]$$

This can be seen from the following derivation. At iteration step  $k-1$ , the pressure and velocity are  $P_{k-1}$  and  $V_{k-1}$ , respectively, and they satisfy eqn [48]

$$K V_{k-1} + G P_{k-1} = F \quad [56]$$

At iteration step  $k$ , the updated pressure is  $P_k$  and the velocity  $V_k = V_{k-1} + v$ , where  $v$  is the unknown increment to be determined. Substituting

$P_k$  and  $V_k$  into [48] and considering  $P_k = P_{k-1} + \alpha_k s_k$ ,  $V_k = V_{k-1} + v$ , and [56] lead to

$$K v + \alpha_k G s_k = 0 \quad \text{or} \quad v = -\alpha_k K^{-1} G s_k \quad [57]$$

From [53], it is clear that the velocity increment  $v = -\alpha_k u_k$ , and consequently eqn [55] updates the velocity.

The final algorithm is given in the right column of **Figure 3** (Ramage and Wathen, 1994). The efficiency of this algorithm depends on how efficiently eqn [53] is solved. We note that the choice of conjugate gradient is simply one of a number of possible choices here. Any of the ‘standard’ Krylov subspace methods including biconjugate gradient, GMRES, can, in principle, be developed in the same way using [52]–[54] wherever matrix-vector products involving the inverse of  $K$  are required. Preconditioning for the pressure equation can be of great help in improving the convergence of this iteration, as discussed in Moresi and Solomatov (1995).

It should be pointed out that the Uzawa algorithm outlined above can also be used in connection with other numerical methods including FV and FD methods, provided that the matrix equations for pressure and velocities from these numerical methods have the form of [37].

#### 7.05.4.1.4 Multigrid solution strategies

The stiffness matrix  $K$  is symmetric positive definite, and this allows for numerous possible solution approaches. For example, multigrid solvers have

been used for solving eqn [53] (Moresi and Solomatov, 1995) as in Citcom code. Newer versions of Citcom including CitcomS/CitcomCU employ full multigrid solvers with a consistent projection scheme for eqn [53] and are even more efficient (Zhong *et al.*, 2000).

The multigrid method works by formulating the FE problem on a number of different scales – usually a set of grids which are nested one within the other sharing common nodes (see **Figure 4(a)**), similar to how multigrid methods are used in FD and FV methods. The solution progresses on all of the grids at the same time with each grid eliminating errors at a different scale. The effect is to propagate information very rapidly between different nodes in the grid which would otherwise be prevented by the local support of the element shape functions. In fact, by a single traverse from fine to coarse grid and back, all nodes in the mesh can be directly connected to every other – allowing nodes which are physically coupled but remote in the mesh to communicate directly during each iteration cycle. This matches the physical structure of the Stokes flow problem in which stresses are transmitted instantaneously to all parts of the system in response to changes anywhere in the buoyancy forces or boundary conditions.

The multigrid effect relies upon using an iterative solver on each of many nested grid resolutions which acts like a smoother on the residual error at the characteristic scale of that particular grid. Gauss–Seidel iteration is a very common choice because it has exactly this property, although its effectiveness depends on the order in which degrees of freedom are visited by the solver and, consequently, it can be difficult to implement in parallel. On the coarsest grid it is possible to use a direct solver because the number of elements is usually very small.

For an elliptic operator such as the stiffness matrix,  $K$ , of the Stokes flow problem in eqn [53] we write

$$K_b v_b = F_b \quad [58]$$

where the  $b$  subscript indicates that the problem has been discretized to a mesh of fineness  $b$ . An initial estimate of the velocity on grid  $b$ ,  $v_b$ , can be improved by a correction  $\Delta v_b$  determining the solution to

$$K_b \Delta v_b = F_b - K_b v_b \quad [59]$$

Suppose we obtain our approximate initial estimate by solving the problem on a coarse grid. The reduction of the number of degrees of freedom leads to a more manageable problem which can be solved quickly. The correction term is therefore

$$K_b \Delta v_b = F_b - K_b R_b^H v_H \quad [60]$$

where  $H$  indicates a coarser level of discretization, and the operator  $R_b^H$  is an interpolation from the coarse-level  $H$  to the fine-level  $b$ .

To find  $v_H$  we need to solve a coarse approximation to the problem

$$K_H v_H = F_H \quad [61]$$

where  $K_H$  and  $F_H$  are the coarse-level equivalent of the stiffness matrix and force vector. One obvious way to define these is to construct them from a coarse representation of the problem on the mesh  $H$  exactly as would be done on  $b$ . An alternative is to define

$$K_H = R_H^b K_b R_b^H \quad \text{and} \quad F_H = R_H^b F_b \quad [62]$$

where  $R_b^H$  is a ‘restriction’ operator which has the opposite effect to the interpolation operation in that it lumps nodal contributions from the fine mesh onto the coarse mesh.

The power of the algorithm is in a recursive application. The coarse-grid correction is also

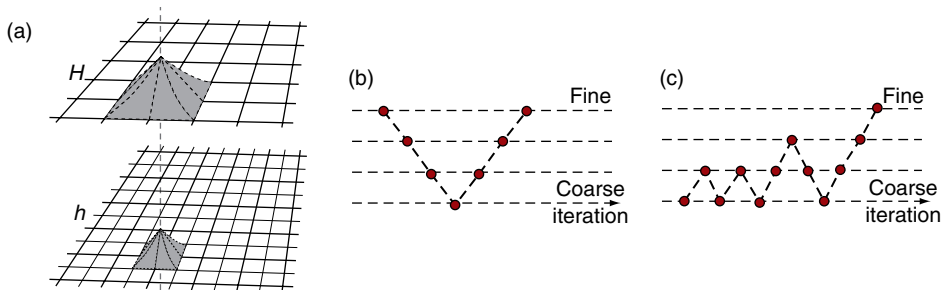


**Figure 4** A nested grids with fine and coarse meshes (a), structure of V cycle multigrid iteration (b) and structure of a full multigrid Iteration (c).

Obtain an approximate solution  $v_h$  at the finest grid,  $h$   
Calculate residual  $r_h = F_h - K_h v_h$   
Project residual by  $N$  levels to  $h-N$   
repeat:  $r_{h-i} = R_{h-i}^{h-(i-1)} r_{h-i-1}$   
Solve exactly  
 $\Delta v_{h-N} = K_{h-N}^{-1} r_{h-N}$   
Interpolate and improve  
 $r_{h-(i-1)} = R_{h-(i-1)}^{h-i} K_{h-i} \Delta v_{h-i}$   
Improve  $\Delta v_{h-(i-1)}$   
 $v_{h-(i-1)} = v_{h-(i-1)} + \Delta v_{h-(i-1)}$

**Figure 5** A simple sawtooth multigrid algorithm for solving eqn [51].

calculated through the use of a still coarser grid and so on, until the problem is so small that an exact solution can be obtained very rapidly. One very simple, but instructive, algorithm for hierarchical residual reduction is the sawtooth cycle given in Figure 5, and its logical layout is same as the V-cycle in Figure 4(b).

The step in which the velocity correction is ‘improved’ is an iterative method for reducing the residual at the current level which has the property of smoothing the error strongly at the current mesh scale. At each level these smoothing operators reduce the residual most strongly on the scale of the discretization – the hierarchical nesting of different mesh sizes allows the residual to be reduced at each scale very efficiently (see Yavneh (2006) for a more lengthy discussion).

The projection and interpolation operators have to be chosen fairly carefully to avoid poor approximations to the problem at the coarse levels and ineffectual corrections propagated to the fine levels. The interpolation operator is defined naturally from the shape functions at the coarse levels. The projection operator is then defined to complement this choice (the operators should be adjoint).

The sawtooth cycle outlined in this section is the simplest multigrid algorithm. Developments include improving the residual at each level of the restriction as well as the interpolation, known as a ‘v-cycle’, and cycles in which the residual is interpolated only part way through the hierarchy before being reprojected and subjected to another set of improvements (a ‘w-cycle’).

The full multigrid algorithm introduces a further level of complexity. Instead of simply casting the problem at a single level and projecting/improving

the residual on a number of grids, the whole problem is defined for all the grids. In this way the initial fine-grid approximation is obtained by interpolating from the solution to the coarsest-grid problem. The solution at each level is still obtained by projecting to the finest level and reducing the residual at each projection step. The resulting cycle is illustrated in Figure 4(c).

A recent overview of multigrid methods is required reading at this point. Yavneh (2006) introduces the method which is then explained for a number of relevant examples by Oosterlee and Gaspar-Lorenz (2006), Bergen *et al.* (2006), and Bastian and Wieners (2006).

#### 7.05.4.2 Stokes Flow: A Penalty Formulation

For 2-D problems, an efficient method to solve the incompressible Stokes flow is a penalty formulation with a reduced and selective integration. This method has been widely used in 2-D thermal convection problems, for example, in ConMan (King *et al.*, 1990). We now briefly discuss this penalty formulation, and detailed descriptions can be found in Hughes (2000).

The key feature in the penalty formulation is to allow for slight compressibility or  $u_{k,k} \approx 0$ . Here it is helpful to make an analogy to isotropic elasticity. The constitutive equations for both compressible and incompressible isotropic elasticity are given by the following two equations:

$$\sigma_{ij} = -P\delta_{ij} + \eta(u_{i,j} + u_{j,i}) \quad [63]$$

$$u_{k,k} + P/\lambda = 0 \quad [64]$$

where  $\lambda$  is the Lame constant which is finite for compressible media but infinite for incompressibility media (i.e., to satisfy  $u_{k,k} = 0$  for finite  $P$ ). To allow for slight compressibility,  $\lambda$  is taken finite but significantly larger than  $\eta$ , such that the error associated with the slight compressibility is negligibly small. Using words of 64 bit long (i.e., double precision),  $\lambda/\eta \sim 10^7$  is effective. For finite  $\lambda$ , the constitutive equation becomes

$$\sigma_{ij} = \lambda u_{k,k} \delta_{ij} + \eta(u_{i,j} + u_{j,i}) \quad [65]$$

which replaces eqn [4].

An interesting consequence of this new constitutive equation is that the pressure is no longer needed in the momentum equation, and this simplifies the

FE analysis. The weak form of the resulting Stokes flow problem is

$$\int_{\Omega} w_{i,j} c_{ijkl} v_{k,l} d\Omega = \int_{\Omega} w_i f_i d\Omega + \sum_{i=1}^{n_{sd}} \int_{\Gamma_{b_i}} w_i b_i d\Gamma - \int_{\Omega} w_{i,j} c_{ijkl} g_{k,l} d\Omega \quad [66]$$

where

$$c_{ijkl} = \lambda \delta_{ij} \delta_{kl} + \eta (\delta_{ik} \delta_{jl} + \delta_{il} \delta_{jk}) \quad [67]$$

The FE implementation of eqn [66] is similar to that in Section 7.05.4.1. With the pressure excluded as a primary variable, the matrix equation is simply

$$[K]\{V\} = \{F\} \quad [68]$$

While the elemental force vector is defined the same as that in [44], the elemental stiffness needs some modification in comparison with that in [42]:

$$k_{lm}^e = \mathbf{e}_i^T \left( \int_{\Omega^e} B_a^T D B_b d\Omega + \int_{\Omega^e} B_a^T \bar{D} B_b d\Omega \right) \mathbf{e}_j \quad [69]$$

where the first integral is the same as in [42] but the second integral is a new addition with

$$\bar{D} = \begin{bmatrix} \lambda & \lambda & 0 \\ \lambda & \lambda & 0 \\ 0 & 0 & 0 \end{bmatrix} \quad [70]$$

The matrix eqn [68] only yields correct solution for velocities if a reduced and selective integration scheme is used to evaluate the elemental stiffness matrix (e.g., Hughes, 2000). Specifically, the numerical quadrature scheme for the second integral of eqn [69] needs to be one order lower than that used for the first integral. For example, if for a 2-D problem, a  $2 \times 2$  Gaussian quadrature scheme is used to evaluate the first integral, then a one-point Gaussian quadrature scheme is needed for the second integral. Hughes (2000) discussed the equivalence theorem for the mixed elements and the penalty formulation with the reduced and selective integration. Moresi *et al.* (1996) showed that these two formulations yield essentially identical results for the Stokes flow problems by comparing solutions from ConMan code employing a penalty formulation and Citcom which uses a mixed formulation.

Finally, we make two remarks about this penalty formulation.

First, although the pressure is not directly solved from the matrix equation, the pressure can be obtained through postprocessing via  $P = -\lambda u_{k,k}$  for each element. Such obtained pressure fields often display a checkerboard pattern. However, a pressure-smoothing scheme (Hughes, 2000) seems to work well. The pressure field is important in many geophysical applications including computing dynamic topography and melt migration.

Second, with  $\lambda/\eta \sim 10^7$ , the stiffness matrix is not well conditioned and is not suited for any iterative solvers. A direct solver is required for this type of equations, as done in ConMan. This implies that this formulation may not be applicable to 3-D problems because of the memory and computation requirements associated with direct solvers. Reducing  $\lambda/\eta$  improves the condition for the stiffness matrix; however, this is not recommended as it results in large errors associated with relaxing the incompressibility constraints.

#### 7.05.4.3 The SUPG Formulation for the Energy Equation

The convective transport of any quantity at high Peclet number (the ratio of advective transport rate to diffusion rate) is challenging in any numerical approach in which the grid does not move with the material deformation. The transfer of quantities from grid points to integration points in order to calculate their updated values introduces a nonphysical additional diffusion term. Furthermore, the advection operator is difficult to stabilize and many different schemes have been proposed to treat grid-based advection in both an accurate and stable fashion. Many of the successful approaches include some attempt to track the flow direction and recognize that the advection operator is not symmetric in the upstream/downstream directions. This section introduces an SUPG formulation and a predictor–multicorrector explicit algorithm for time-dependent energy equation (i.e., eqn [3]). This method was developed by Hughes (2000) and Brooks (1981) some twenty years ago and remains an effective method in FE solutions of the equations with advection and diffusion such as our energy equation. FE mantle convection codes Citcom and ConMan both employ this method for solving the energy equation.

A weak-form formulation for the energy equation [3] and boundary conditions [7] is (Brooks, 1981)

$$\begin{aligned} & \int_{\Omega} w(\dot{T} + u_i T_{,i}) d\Omega + \int_{\Omega} w_{,i}(\kappa T_{,i}) d\Omega \\ & + \sum_e \int_{\Omega_e} \bar{w}[\dot{T} + u_i T_{,i} - (\kappa T_{,i})_{,i} - \gamma] d\Omega \\ & = \int_{\Omega} w\gamma d\Omega + \int_{\Gamma_q} wq d\Gamma - \int_{\Omega} w_{,i}\kappa g_i d\Omega \end{aligned} \quad [71]$$

where  $w$  is the regular weighting functions and is zero on  $\Gamma_q$ ,  $\dot{T}$  is the time derivative of temperature, and  $\bar{w}$  is the streamline upwind contribution to the weighting functions.

The FE implementation of [71] is similar to what was discussed for the Stokes flow in Section 7.05.4.1.2. While the weighting function  $w$  is similar to what was defined in [39] except it is now a scalar, the streamline upwind part  $\bar{w}$  is defined through artificial diffusivity  $\tilde{\kappa}$  as

$$\bar{w} = \tilde{\kappa} \hat{u}_j w_j / |u| \quad [72]$$

where  $|u|$  is the magnitude of flow velocity,  $\hat{u}_j = u_j / |u|$  represents the directions of flow velocity, and  $\tilde{\kappa}$  is defined as

$$\tilde{\kappa} = \left( \sum_{i=1}^{n_{sd}} \xi_i u_i b_i \right) / 2 \quad [73]$$

$$\xi_i = \begin{cases} -1 - 1/\alpha_i, & \alpha_i < -1 \\ 0, & -1 \leq \alpha_i \leq 1, \text{ for } \alpha_i = \frac{u_i b_i}{2\kappa} \\ 1 - 1/\alpha_i, & \alpha_i > 1 \end{cases} \quad [74]$$

where  $u_i$  and  $b_i$  are flow velocity and element lengths in certain directions. It should be pointed out that eqns [72] and [74] are empirical and other forms are possible. Such defined streamline upward weighting function  $\bar{w}$  can be thought as adding artificial diffusion to the actual diffusion term to lead to total diffusivity

$$\kappa + \tilde{\kappa} \hat{u}_i \hat{u}_j \quad [75]$$

$\bar{w}$  is discontinuous across elemental boundaries, different from  $w$ . This is why the integral in the third term of [72] is for each element.  $\bar{w} = w + \bar{w}$  is also sometimes called the Petrov–Galerkin weighting functions which indicates that the shape function used to weight the integrals and the shape function for interpolation are distinct.

A reasonable assumption is the weighted diffusion for an element in the third term of eqn [71],  $\bar{w}(\kappa T_{,i})_{,i}$ , is negligibly small. Therefore, eqn [71] can be written as

$$\begin{aligned} & \int_{\Omega} w_{,i}(\kappa T_{,i}) d\Omega + \sum_e \int_{\Omega_e} \bar{w}(\dot{T} + u_i T_{,i} - \gamma) d\Omega \\ & = \int_{\Gamma_q} wq d\Gamma - \int_{\Omega} w_{,i}\kappa g_i d\Omega \end{aligned} \quad [76]$$

We now present relevant matrices at an element level. The  $\dot{T}$  term in [71] implies that a mass matrix is needed and it is given as

$$m_{ab}^e = \int_{\Omega^e} N_a N_b d\Omega \quad [77]$$

where  $a, b = 1, \dots, n_{en}$ . Elemental stiffness  $k^e$  is

$$k_{ab}^e = \int_{\Omega^e} B_a^T \kappa B_b d\Omega \quad [78]$$

where for 2-D problems

$$B_a^T = (N_{a,1} \ N_{a,2}) \quad [79]$$

Elemental force vector  $f^e$  is given as

$$f^e = \int_{\Omega^e} \tilde{N}_a \gamma d\Omega + \int_{\Gamma_q^e} \tilde{N}_a q d\Gamma - \sum_{b=1}^{n_{en}} k_{ab}^e g_b^e \quad [80]$$

where  $\tilde{N}_a$  is the Petrov–Galerkin shape function.

Elemental advection matrix  $c^e$  is given as

$$c_{ab}^e = \int_{\Omega^e} \tilde{N}_a u_i N_{b,i} d\Omega \quad [81]$$

The combined matrix equation may be written as

$$M \dot{\Phi} + (K + C)\Phi = F \quad [82]$$

where  $\Phi$  is the unknown temperature, and  $M$ ,  $K$ ,  $C$ , and  $F$  are the total mass, stiffness, advection matrices, and force vector assembled from all the elements.

Equation [82] can be solved using a predictor–corrector algorithm (Hughes, 2000) with some initial condition for temperature (e.g., eqn [5]). Suppose that temperature and its time derivative at time step  $n$  are given,  $\Phi_n$  and  $\dot{\Phi}_n$ , the solutions at time step  $n+1$  with time increment  $\Delta t$  can be obtained with the following algorithm:

1. Predictor:

$$\begin{aligned} \Phi_{n+1}^0 &= \Phi_n + \Delta t(1-\alpha)\dot{\Phi}_n, \quad \dot{\Phi}_{n+1}^0 = 0, \\ & \text{iteration step } i = 0 \end{aligned} \quad [83]$$

2. Solving:

$$M^* \Delta \dot{\Phi}_{n+1}^i = \prod_e (f_{n+1}^e - m^e \dot{\Phi}_{n+1}^i - (k^e + c^e) \Phi_{n+1}^i) \quad [84]$$

3. Corrector:

$$\Phi_{n+1}^{i+1} = \Phi_{n+1}^i + \Delta t \alpha \Delta \dot{\Phi}_{n+1}^i, \dot{\Phi}_{n+1}^{i+1} = \dot{\Phi}_{n+1}^i + \Delta \dot{\Phi}_{n+1}^i \quad [85]$$

4. If needed, set iteration step  $i = i + 1$  and go back step 2.

We make four remarks for this algorithm. First, this method is second-order accurate if  $\alpha = 0.5$  (Hughes, 2000). Second, typically two iterations are sufficient. Third, in [84]  $\prod$  represents the operation of assembling elemental matrix into global matrix, and  $M^*$  is the lumped mass matrix which essentially makes this scheme an explicit scheme. Fourth, time increment  $\Delta t$  needs to satisfy Courant time-stepping constraints to make the scheme stable (Hughes, 2000).

### 7.05.5 Incorporating More Realistic Physics

In Section 7.05.2, we presented the governing equations for thermal convection in a homogeneous incompressible fluid with a Newtonian (linear) rheology and the Boussinesq approximation. However, the Earth's mantle is likely much more complicated with heterogeneous composition and non-Newtonian rheology (*see* Chapter 7.02). In addition, non-Boussinesq effects such as solid–solid phase transitions may play an important role in affecting the dynamics of the mantle. In this section, we will discuss the methods that help incorporate these more realistic physics in studies of mantle convection. We will focus on modeling thermochemical convection, solid-state phase transitions, and non-Newtonian rheology.

#### 7.05.5.1 Thermochemical Convection

Thermal convection for a compositionally heterogeneous mantle has gained a lot of interest in recent years (Lenardic and Kaula, 1993; Tackley, 1998a; Davaille, 1999; Kellogg *et al.*, 1999; Chapter 7.10), with focus on the roles of mantle compositional anomalies and crustal structure in mantle dynamics. This is also called thermochemical convection. Different from purely thermal convection for which the fluid has the same composition, thermochemical convection involves fluids with different compositions.

Here we will present governing equations and numerical methods for solving these equations (*see also* Chapters 7.02 and 7.10).

##### 7.05.5.1.1 Governing equations

Governing equations for thermochemical convection include a transport equation that describes the movement of compositions, in addition to the conservation laws of the mass, momentum, and energy (i.e., eqns [1]–[3]). Suppose that  $C$  describes the compositional field, the transport equation is

$$\frac{\partial C}{\partial t} + u_i C_{,i} = 0 \quad [86]$$

This transport equation is similar to the energy equation [3] except that chemical diffusion and source terms are ignored, which is justified given that chemical diffusion is likely extremely small for the length- and timescales that we consider in mantle convection. For a two-component system such as the crust–mantle system or depleted-primordial mantle system,  $C$  can be either 0 or 1, representing either component. If the fluids of different compositions have intrinsically different density, then the momentum eqn [2] needs to be modified to take into account the compositional effects on the buoyancy

$$\sigma_{ij,j} + Ra(T - \beta C)\delta_{iz} = 0 \quad [87]$$

where  $\beta$  is the buoyancy number (van Keken *et al.*, 1997; Tackley and King, 2003) and is defined as

$$\beta = \Delta\rho / (\rho\Delta T\alpha) \quad [88]$$

where  $\Delta\rho$  is the density difference between the two compositions,  $\rho$  and  $\Delta T$  are the reference density and temperature, and  $\alpha$  is the reference coefficient of thermal expansion.

A special class of thermochemical convection problems examine how the mantle compositional heterogeneity is stirred by mantle convection (e.g., Gurnis and Davies, 1986; Christensen, 1989; Kellogg, 1992; van Keken and Zhong, 1999). For these studies on the mixing of the mantle, we may assume that the fluids with different compositions have identical density with  $\beta = 0$ .

##### 7.05.5.1.2 Solution approaches

Solving the conservation equations of the mass, momentum, and energy for thermochemical convection is identical to what was introduced in Section 7.05.3 for purely thermal convection. The additional compositional buoyancy term in the momentum equation [87] does not present any new difficulties

numerically, provided that the composition  $C$  is given. The new challenge is to solve the transport equation [86] effectively.

A number of techniques have been developed or adapted in solving the transport equation in thermochemical convection studies. They include a field method with a filter (e.g., Hansen and Yuen, 1988; Lenardic and Kaula, 1993), a marker chain method (Christensen and Yuen, 1984; van Keken *et al.*, 1997; Zhong and Hager, 2003), and a particle method (e.g., Weinberg and Schmeling, 1992; Tackley, 1998a; Tackley and King, 2003; Gerya and Yuen, 2003). As reviewed by van Keken *et al.* (1997), while these techniques work to some extent, they also have their limitations, particularly in treating entrainment and numerical diffusion of composition  $C$ . We will briefly discuss each of these methods with more emphasis on the particle method.

In the particle method, the transport equation for  $C$  (i.e., eqn [86]) is not solved directly. Composition  $C$  at a given time is represented by a set of particles. This representation requires a mapping from the distribution of particles to compositional field  $C$  which is often represented on a numerical mesh. With the mapping, to update  $C$ , all that is needed is to update the position of each particle to obtain an updated distribution of particles. This effectively solves the transport equation for  $C$ .

Two different particle methods have been used to map distribution of particles to  $C$ : absolute and ratio methods (Tackley and King, 2003). In the absolute method, particles are only used to represent one type of composition (e.g., for dense component or with  $C = 1$ ). The population density of particles can be mapped to  $C$ . For example,  $C$  for an element/grid cell with volume  $\Omega_e$  and particles  $N_e$  can be given as

$$C_e = AN_e / \Omega_e \quad [89]$$

where the constant  $A$  is the reciprocal of initial density of particles for composition  $C=1$  (i.e., total number of particles divided by the volume of composition  $C=1$ ). Clearly, the absence of particles in an element/grid cell represents  $C=0$ . A physically unrealistic situation with  $C>1$  may arise due to statistical fluctuations in particle distribution or particle settling. Therefore, for this method to work effectively, a large number of particles are required (Tackley and King, 2003).

In the ratio method, two different types of particles are used to represent the compositional field  $C$ , type 1 for  $C=0$  and type 2 for  $C=1$ .  $C$  for an

element/grid cell that includes type 1 particles  $N_1$  and type 2 particles  $N_2$  is given as

$$C_e = N_2 / (N_1 + N_2) \quad [90]$$

In the ratio method,  $C$  can never be greater than 1. Tackley and King (2003) found that the ratio method is particularly effective in modeling thermochemical convection in which the two components occupy similar amount of volumes.

We now discuss briefly procedures to update the positions of particles. One commonly used method is a high-order Runge–Kutta method (e.g., van Keken *et al.*, 1997). Here we present a predictor–corrector scheme for updating the particle positions (e.g., Zhong and Hager, 2003). Suppose that at time  $t = t_0$ , flow velocity is  $\mathbf{u}_0$  and compositional field is  $C_0$  that is defined by a set of particles with coordinates,  $\mathbf{x}_0^i$ , for particle  $i$ . The algorithm for solving composition at the next time step  $t = t_0 + dt = t_1$ ,  $C_1$ , can be summarized as follows:

1. Using a forward Euler scheme, predict the new position for each particle  $i$  with  $\mathbf{x}_{1p}^i = \mathbf{x}_0^i + \mathbf{u}_0 dt$  and mapping the particles to compositional field  $C_{1p}$  at  $t = t_1$ .
2. Using the predicted  $C_{1p}$ , solve the Stokes equation for new velocity  $\mathbf{u}_{1p}$ .
3. Using a modified Euler scheme with second-order accuracy, compute the position for each particle  $i$  with  $\mathbf{x}_1^i = \mathbf{x}_0^i + 0.5(\mathbf{u}_0 + \mathbf{u}_{1p})dt$  and compositional field  $C_1$  at  $t = t_1$ .

The marker chain method is similar to the particle method in a number of ways. In the marker chain method, composition  $C$  is defined by an interfacial boundary that separates two different components. The interfacial boundary is a line for 2-D problems or a surface for 3-D. Using the flow velocity, one tracks the evolution of the interfacial boundary and hence composition  $C$ . Often the interfacial boundary is represented by particles or markers. Therefore, updating the interfacial boundary is essentially the same as updating the particles in the particle method. Composition  $C$  on a numerical grid which is desired for solving the momentum and energy equations [87] and [3] can be obtained by projection. As van Keken *et al.* (1997) indicated, the marker chain method is rather effective for compositional anomalies with relatively simple structure and geometry in 2-D.

The field method is probably the most straightforward. By setting diffusivity to be zero, we can employ the same solver for the energy equation (e.g., in

Section 7.05.4.3) to solve the transport equation for  $C$ . However, this often introduces numerical artifacts including numerical oscillations and numerical diffusion. Lenardic and Kaula (1993) introduced a filter scheme that removes the numerical oscillations while conserving the total mass of compositional field.

### 7.05.5.2 Solid-State Phase Transition

Solid-state phase transitions are important phenomena in the mantle. Major phase transitions include olivine–spinel transition at 410 km depth and spinel-to-perovskite and magnesium-to-wustite transitions at 670 km depth, that are associated with significant changes in mantle density and seismic wave speeds. Recently, it was proposed that the D'' discontinuity near the core–mantle boundary is also caused by a phase transition from perovskite to post-perovskite (Murakami, *et al.*, 2004). These phase transitions may affect the dynamics of mantle convection in two ways: (1) on the energetics due to latent heating associated with phase transitions, (2) on the buoyancy due to undulations at phase boundary caused by lateral variations in mantle temperature that affects the pressure at which phase transitions occur (Richter, 1973; Schubert *et al.*, 1975; Christensen and Yuen, 1985; Tackley *et al.*, 1993; Zhong and Gurnis, 1994). In this section, following Richter (1973) and Christensen and Yuen (1985), we present a method to model phase transitions.

The undulations of a phase boundary represent additional buoyancy force that affects the momentum equation. For phase transition  $k$  with density change  $\Delta\rho_k$ , the phase boundary undulations for phase transition  $k$  with density change  $\Delta\rho_k$  can be described by a dimensionless phase-change function  $\Gamma_k$  that varies from 0 to 1 where regions with  $\Gamma_k$  of 0 and 1 represent the two phases separated by this phase-change boundary. The momentum equation can be written as

$$\rho_{ij,j} + (RaT - \sum_k Ra_k \Gamma_k) \delta_{iz} = 0 \quad [91]$$

where phase-change Rayleigh number  $Ra_k$  is

$$Ra_k = \frac{\Delta\rho_k g D^3}{\kappa \eta_0} \quad [92]$$

The phase-change function  $\Gamma_k$  is defined via ‘excess pressure’

$$\pi_k = P - P_0 - \gamma_k T \quad [93]$$

where  $\gamma_k$  and  $P_0$  are the Clapeyron slope and phase-change pressure at zero-degree temperature for the

$k$ th phase transition. After normalizing pressure by  $\rho_0 gD$  and Clapeyron slope by  $\rho_0 gD/\Delta T$ , the nondimensional ‘excess pressure’ can be written as

$$\pi_k = 1 - d_k - z - \gamma_k(T - T_k) \quad [94]$$

where  $\gamma_k$ ,  $d_k$ , and  $T_k$  are the nondimensional Clapeyron slope, reference-phase transition depth, and reference-phase transition temperature for the  $k$ th phase transition, respectively. The dimensionless phase-change function is then given as

$$\Gamma_k = \frac{1}{2} \left( 1 + \tanh \frac{\pi_k}{d} \right) \quad [95]$$

where  $d$  is dimensionless phase transition width which measures the depth segment over which the phase change occurs. It should be pointed out that the effect of phase transition on buoyancy force can also be modeled with ‘effective’ coefficient of thermal expansion (Christensen and Yuen, 1985).

The latent heating effect, along with viscous heating and adiabatic heating, can be included in the energy equation (also see eqn [3]) as (Christensen and Yuen, 1985)

$$\begin{aligned} & \left[ 1 + \sum_k \gamma_k^2 \frac{Ra_k}{Ra} \frac{d\Gamma_k}{d\pi_k} D_i (T + T_s) \right] \left( \frac{\partial T}{\partial t} + \mathbf{v} \cdot \nabla T \right) \\ & + \left( 1 + \sum_k \gamma_k \frac{Ra_k}{Ra} \frac{d\Gamma_k}{d\pi_k} \right) (T + T_s) D_i v_z \\ & = \nabla^2 T + \frac{D_i}{Ra} \tau_{ij} \frac{\partial v_i}{\partial x_j} + \gamma \end{aligned} \quad [96]$$

where  $T_s$ ,  $v_z$ , and  $\tau_{ij}$  are the surface temperature, vertical velocity, and deviatoric stress, respectively;  $k$  is phase-change index;  $D_i$  is the dissipation number and is defined as

$$D_i = \frac{\alpha g D}{C_p} \quad [97]$$

where  $\alpha$  and  $C_p$  are the coefficient of thermal expansion and specific heat (see also Chapter 7.02). Christensen and Yuen (1985) called the effects of latent heating, viscous heating, and adiabatic heating as non-Boussinesq effects and termed this formulation as extended-Boussinesq formulation. They suggest that these effects are all of similar order, proportional to  $D_i$ , and should be considered simultaneously.

The modified momentum and energy equations [91] and [96] can be solved with the same algorithms such as the Uzawa and SUPG for mantle convection

problems with extended-Boussinesq approximations in 3-D (e.g., Zhong, 2006; Kameyama and Yuen, 2006).

### 7.05.5.3 Non-Newtonian Rheology

Laboratory studies suggest that the deformation of olivine, the main component in the upper mantle, follows a power-law rheology (e.g., Karato and Wu, 1993):

$$\dot{\varepsilon} = A\tau^n \quad [98]$$

where  $\dot{\varepsilon}$  is the strain rate,  $\tau$  is the deviatoric stress, the pre-exponent constant  $A$  represents other effects such as grain size and water content, and the exponent  $n$  is  $\sim 3$ . The nonlinearity in the rheology arises from  $n \neq 1$  (*see also* Chapter 7.02).

The effects of non-Newtonian rheology on mantle convection were first investigated by Parmentier *et al.* (1976) and Christensen (1984). More recent efforts have been focused on how non-Newtonian rheology including viscoplastic rheology may lead to dynamic generation of plate tectonics (King and Hager, 1990; King *et al.*, 2002; Bercovici, 1995; Moresi and Solomatov, 1998; Zhong *et al.*, 1998; Tackley, 1998b; Trompert and Hansen, 1998).

Solutions of nonlinear problems in general require an iterative approach. The power-law rheology may be written as an expression for effective viscosity

$$\sigma_{ij} = -P\delta_{ij} + 2\eta_{\text{eff}}\dot{\varepsilon}_{ij} \quad [99]$$

$$\eta_{\text{eff}} = \tau/\dot{\varepsilon} = \frac{1}{A}\dot{\varepsilon}^{(1-n)/n} \quad [100]$$

where  $\dot{\varepsilon}$  is the second invariant of strain-rate tensor

$$\dot{\varepsilon} = \left( \frac{1}{2}\dot{\varepsilon}_{ij}\dot{\varepsilon}_{ij} \right)^{1/2} \quad [101]$$

It is clear that the effective viscosity depends on strain rate which in turn depends on flow velocity. Therefore, a general strategy for this problem is (1) starting with some guessed effective viscosity, solve the Stokes flow problem for flow velocities; (2) update the effective viscosity with the newly determined strain rate, and solve the Stokes flow again; (3) keep this iterative process until flow velocities are convergent.

Implementation of this iterative scheme is straightforward. The convergence for this iterative process depends on the exponent  $n$ . For regular power-law rheology with  $n \sim 3$ , convergence is usually not a problem. However, for large  $n$  (e.g., in case of viscoplastic rheology), the iteration may

converge very slowly or may diverge. Often some forms of damping may help improve convergence significantly (e.g., King and Hager, 1990).

### 7.05.6 Concluding Remarks and Future Prospects

In this chapter, we have discussed four basic numerical methods for solving mantle convection problems: FE, FD, FV, and spectral methods. We have focused our efforts on FE method, mainly because of its growing popularity in mantle convection studies over the past decade, partially prompted by the easily accessed FE codes from Conman to Citcom. To this end, the discussions on FE method should help readers understand the inner working of these two FE codes. However, our discussions on FD, FV, and spectral methods are rather brief and are meant to give readers a solid basis for understanding the rudiments of these methods and the references with which to delve deeper into the subjects. These three methods have all been widely used in studies of mantle convection and will most likely remain so for years to come. It is our view that each of these methods has its advantages and disadvantages and readers need to find the one that is most suited to their research. This chapter is by no means exhaustive or extremely advanced in character. We did not cover many potentially interesting and powerful numerical techniques, such as spectral elements (e.g., Komatitsch and Tromp, 1999), wavelets (Daubeshies *et al.*, 1985), level-set method (Osher and Fedkiew, 2003), and adaptive grid techniques (Berger and Oliger 1984; Bruegmann and Tichy, 2004), and interested readers can read these references to learn more.

Rapid advancement in computing power has made 3-D modeling of mantle convection practical, although 2-D modeling still plays an essential role. While a variety of solvers with either iterative or direct solution method are available to 2-D models, 3-D modeling requires iterative solution techniques due to both computer memory and computational requirements. A powerful iterative solution approach is the multigrid method that can be used in either FE or FV method. Such methods are already implemented in a number of mantle convection codes including STAG3D (Tackley, 1994), Citcom/CitcomS (Moresi and Solomatov, 1995; Zhong *et al.*, 2000), and Terra (Baumgardner, 1985). We spent some effort in discussing the multigrid method, and more on this topic can be found in Brandt (1977), Trottenberg *et al.* (2001),

and Yavneh (2006). The multigrid idea is powerful in that one can generalize this to structures other than grids, for instance multiscale or multilevel techniques (Trottenberg *et al.*, 2001).

Three-dimensional modeling should almost certainly make a good use of parallel computing with widely available parallel computers from PC-clusters to super-parallel computers. Parallel computing technology poses certain limitations on numerical techniques as well. For example, spectral methods, while having some important advantages over other grid-based numerical methods, are much more difficult to implement efficiently in parallel computing. This may severely limit its use to tackle next-generation computing problems. Fortunately, many other numerical methods including FE, FD, and FV methods are very efficient for parallel computing. Many of the codes mentioned earlier for mantle convection studies including STAG3D, Citcom/CitcomS, Terra, and those in Harder and Hansen (2005) and Kageyama and Sato (2004) are fully parallelized and can be used on different parallel computers. These codes can be scaled up to possibly thousands of processors with a great potential yet to be explored in helping understand high-resolution, high-Rayleigh-number mantle convection.

However, there remain many challenges in numerical modeling of mantle convection, both in developing more robust numerical algorithms and in analyzing model results. At least four areas need better numerical algorithms. (1) Thermochemical convection becomes increasingly important in answering a variety of geodynamic questions. We discussed cursorily a Lagrangian technique of advection of tracers in solving thermochemical convection. However, it is clear that most existing techniques do not work well for entrainment in thermochemical convection, as demonstrated by van Keken *et al.* (1997) and Tackley and King (2003). The increasing computing power will help solve this problem by providing significantly high resolution, but better algorithms are certainly needed. (2) The lithosphere is characterized by highly nonlinear rheology including complex shear-localizing feedback mechanisms and history-dependent rheology and plastic deformation (Gurnis *et al.*, 2000; Bercovici, 2003). Convergence deteriorates rapidly when nonlinearity increases. More robust algorithms are needed for solving mantle convection with highly nonlinear rheology. (3) Robust algorithms are needed in order to incorporate compressibility in mantle convection and to better compare with seismic and

mineral physics models. 2-D compressible mantle convection models with simple thermodynamics have been formulated (Jarvis and McKenzie, 1980; Ita and King, 1998). We anticipate more developments in the near future. (4) Multiscale physics is an important feature of mantle convection. Earth's mantle convection is of very long wavelengths, for example,  $\sim 10\,000$  km for the Pacific Plate. However, mantle convection is also fundamentally controlled by thin thermal boundary layers that lead to thin upwelling plumes ( $\sim 100$  km) and downwelling slabs due to high Rayleigh number in mantle convection. Plate boundary processes and entrainment in thermochemical convection also occur over possibly even smaller length scale. Furthermore, material properties are also affected by near-microscopic properties such as grain size, which has not been well incorporated in mantle convection studies. Most existing numerical methods in mantle convection work for largely uniform grids. New methods that work with dynamic adaptive mesh refinement are needed. Finally, it is necessary for all these new methods and algorithms to work efficiently in 2-D/3-D on parallel computers.

Efficient postprocessing and analyses of modeling results are also increasingly becoming an important issue. Mantle convection, along with many other disciplines in the geosciences, now faces an exponential increase in the amount of numerical data generated in large-scale high-resolution 3-D convection. It is currently commonplace to have a few terabytes of data for a single project and this poses significant challenges to conventional ways of data analyses, post-processing, and visualization. Visualization is already a severe problem even in the era of terascale computing. Considering our future quest to the petascale computing, this problem would be greatly exacerbated in the coming decade. It is essential to employ modern visualization tools to confront this challenge. Erlebacher *et al.* (2001) discussed these issues and their solutions, and similar arguments about these problems and their solutions can be found in a report on high-performance computing in geophysics by Cohen (2005). Several potentially useful methodologies such as 2-D/3-D feature extraction, segmentation methods, and flow topology (see Hansen and Johnson, 2005) can help geophysicists understand better the physical structure of time-dependent convection with coherent structures, such as plumes or detached slabs in spherical geometry. 3-D visualization packages, for example, AMIRA or PARAVIEW, can help to

alleviate the burden of the researcher in unraveling the model output. Going further into detailed examination of 3-D mantle convection, one would need large-scale display devices such as the PowerWall with more than 12 million pixels or CAVE-like environments. This particular visualization method is described under current operating conditions in the Earth Simulator Center by Ohno *et al.* (2006). Remote visualization of the data under the auspices of Web-services using the client-server paradigm may be a panacea for collaborative projects (see Erlebacher *et al.*, 2006).

Finally, it is vitally important to develop and maintain efficient and robust benchmarks, as in any fields of computational sciences. Benchmark efforts have been made in the past by various groups for different mantle convection problems (e.g., Blankenbach *et al.*, 1989; van Keken *et al.*, 1997; Tackley, 1994; Moresi and Solomatov, 1995; Zhong *et al.*, 2000; Stemmer *et al.*, 2006). As numerical methods and computer codes become more sophisticated and our community moves into tera- and petascale computing era, benchmark efforts become even more important to assure the efficiency and accuracy.

## References

- Albers M (2000) A local mesh refinement multigrid method for 3-D convection problems with strongly variable viscosity. *Journal of Computational Physics* 160: 126–150.
- Atanga J and Silvester D (1992) Iterative methods for stabilized mixed velocity-pressure finite elements. *International Journal of Numerical Methods in Fluids* 14: 71–81.
- Auth C and Harder H (1999) Multigrid solution of convection problems with strongly variable viscosity. *Geophysical Journal International* 137: 793–804.
- Balachandar S and Yuen DA (1994) Three-dimensional fully spectral numerical method for mantle convection with depth-dependent properties. *Journal of Computational Physics* 132: 62–74.
- Balachandar S, Yuen DA, Reuteler DM, and Lauer G (1995) Viscous dissipation in three dimensional convection with temperature-dependent viscosity. *Science* 267: 1150–1153.
- Bastian P and Wieners C (2006) Multigrid methods on adaptively refined grids. *Computing in Science and Engineering* 8(6): 44–55.
- Bathe K-J (1996) *Finite Element Procedures*, 1037 pp. Englewood Cliffs, NY: Prentice Hall.
- Baumgardner JR (1985) Three dimensional treatment of convectionflow in the Earth's mantle. *Journal of Statistical Physics* 39(5/6): 501–511.
- Bercovici D (2003) The generation of plate tectonics from mantle convection. *Earth and Planetary Science Letters* 205: 107–121.
- Bercovici D (1995) A source-sink model of the generation of plate tectonics from non-Newtonian mantle flow. *Journal of Geophysical Research* 100: 2013–2030.
- Bergen B, Gradi T, Huelsemann F, and Ruede U (2006) A massively parallel multigrid method for finite elements. *Computing in Science and Engineering* 8(6): 56–62.
- Berger M and Oliger J (1984) Adaptive mesh refinement for hyperbolic partial differential equations. *Journal of Computational Physics* 53: 484–512.
- Blankenbach B, Busse F, Christensen U, *et al.* (1989) A benchmark comparison of mantle convection codes. *Geophysical Journal International* 98: 23–38.
- Bollig EF, Jensen PA, Lyness MD, *et al.* (in press) VLAB: Web Services, Portlets, and Workflows for enabling cyber-infrastructure in computational mineral physics. *Physics of the Earth and Planetary Interiors*.
- Brandt A (1999) Multi-level adaptive solutions to boundary-value problems. *Mathematics of Computation* 31: 333–390.
- Briggs WL, Henson VE, and McCormick SF (2000) *A Multigrid Tutorial*, 2nd edn. SIAM Press, 2000.
- Brooks AN and Petrov-Galerkin A (1981) *Finite Element Formulation for Convection Dominated Flows*. PhD Thesis, California Institute of Technology, Pasadena, CA.
- Bruegmann B and Tichy W (2004) Numerical solutions of orbiting black holes. *Physical Review Letters* 92: 211101.
- Bunge HP, Richards MA, Lithgow-Bertelloni C, Baumgardner JR, Grand SP, and Romanowicz BA (1998) Time scales and heterogeneous structure in geodynamic Earth models. *Science* 280: 91–95.
- Bunge H-P, Richards MA, and Baumgardner JR (1997) A sensitive study of 3-dimensional spherical mantle convection at 108 Rayleigh number: Effects of depth-dependent viscosity, heating mode, and an endothermic phase change. *Journal of Geophysical Research* 102: 11991–12007.
- Busse FH (1989) Fundamentals of thermal convection. In: Peltier WR (ed.) *Mantle Convection, Plate Tectonics and Global Dynamics*, pp. 23–109. New York: Gordon and Breach.
- Christensen U (1989) Mixing by time-dependent convection. *Earth and Planetary Science Letters* 95: 382–394.
- Christensen UR (1984) Convection with pressure- and temperature-dependent non-Newtonian rheology. *Geophysical Journal of the Royal Astronomical Society* 77: 343–384.
- Christensen UR and Yuen DA (1985) Layered convection induced by phase changes. *Journal of Geophysical Research* 90: 10291–10300.
- Christensen UR and Yuen DA (1984) The interaction of a subducting lithosphere with a chemical or phase boundary. *Journal of Geophysical Research* 89(B6): 4389–4402.
- Cohen RE (ed.) (2005) *High-Performance Computing Requirements for the Computational Solid-Earth Sciences*, 101 pp. ([http://www.geoprose.com/computational\\_SES.html](http://www.geoprose.com/computational_SES.html)).
- Cserepes L, Rabinowicz M, and Rosenberg-Borot C (1988) Three-dimensional infinite Prandtl number convection in one and two layers with implication for the Earth's gravity field. *Journal of Geophysical Research* 93: 12009–12025.
- Cserepes L and Rabinowicz M (1985) Gravity and convection in a two-layer mantle. *Earth and Planetary Science Letters* 76: 193–207.
- Daubeschies I, Grossmann A, and Meyer Y (1985) Painless nonorthogonal expansions. *Journal of Mathematical Physics* 27: 1271–1283.
- Davaille A (1999) Simultaneous generation of hotspots and superswells by convection in a heterogeneous planetary mantle. *Nature* 402: 756–760.
- Davies GF (1995) Penetration of plates and plumes through the mantle transition zone. *Earth and Planetary Science Letters* 133: 507–516.

- Desai CS and Abel JF (1972) *Introduction to the Finite Element Method. A Numerical Method for Engineering Analysis*. New York: Academic Press.
- Erlebacher C, Yuen DA, and Dubuffet F (2001) Current trends and demands in visualization in the geosciences. *Visual Geosciences* 6: 59 (doi:10.1007/s10069-001-1019-y).
- Erlebacher G, Yuen DA, Lu Z, Bollig EF, Pierce M, and Pallickara S (2006) A grid framework for visualization services in the Earth Sciences. *Pure and Applied Geophysics* 163: 2467–2483.
- Fornberg B (1990) High-order finite differences and the pseudospectral method on staggered grids. *SIAM Journal on Numerical Analysis* 27: 904–918.
- Fornberg BA (1995) *A Practical Guide to Pseudospectral Methods*. Cambridge: Cambridge University Press.
- Gable CW, O'Connell RJ, and Travis BJ (1991) Convection in three dimensions with surface plates: Generation of toroidal flow. *Journal of Geophysical Research* 96: 8391–8405.
- Gerya TV and Yuen DA (in press) Robust characteristics method for modeling multiphase visco-elastoplastic thermo-mechanical problems. *Physics of the Earth and Planetary Interiors*.
- Gerya TV, Connolly JAD, Yuen DA, Gorczyk W, and Capel AM (2006) Seismic implications of mantle wedge plumes. *Physics of the Earth and Planetary Interiors* 156: 59–74.
- Gerya TV and Yuen DA (2003) Characteristics-based marker method with conservative finite-differences schemes for modeling geological flows with strongly variable transport properties. *Physics of the Earth and Planetary Interiors* 140: 295–320.
- Glatzmaier GA (1988) Numerical simulations of mantle convection: Time-dependent, three-dimensional, compressible, spherical shell. *Geophysics and Astrophysics Fluid Dynamics* 43: 223–264.
- Glatzmaier GA and Roberts PH (1995) A three-dimensional self-consistent computer simulation of a geomagnetic field reversal. *Nature* 377: 203–209.
- Golub GH and van Loan CF (1989) *Matrix Computations*, 642 pp. Baltimore, MD: The Johns Hopkins University Press.
- Griffiths DV and Smith IM (2006) *Numerical Methods for Engineers*, 2nd edn. New York: Chapman and Hall.
- Gurnis M, Zhong S, and Toth J (2000) On the competing roles of fault reactivation and brittle failure in generating plate tectonics from mantle convection. In: Richards MA, Gordon R, and van der Hilst R (eds.) *The History and Dynamics of Global Plate Motions*, pp. 73–94. Washington, DC: American Geophysical Union.
- Gurnis M and Davies GF (1986) Mixing in numerical models of mantle convection incorporating plate kinematics. *Journal of Geophysical Research* 91: 6375–6395.
- Hackbusch W (1985) *Multigrid Methods and Applications*. Berlin: Springer Verlag.
- Hager BH and Richards MA (1989) Long-wavelength variations in Earth's geoid: Physical models and dynamical implications. *Philosophical Transactions of the Royal Society of London A* 328: 309–327.
- Hager BH and O'Connell RJ (1981) A simple global model of plate dynamics and mantle convection. *Journal of Geophysical Research* 86: 4843–4878.
- Hansen CD and Johnson CR (eds.) (2005) *The Visualization Handbook*, 962 pp. Amsterdam: Elsevier.
- Hansen U and Yuen DA (1988) Numerical simulations of thermal chemical instabilities and lateral heterogeneities at the core–mantle boundary. *Nature* 334: 237–240.
- Harder H and Hansen U (2005) A finite-volume solution method for thermal convection and dynamo problems in spherical shells. *Geophysical Journal International* 161: 522–537.
- Hughes TJR (2000) *The Finite Element Method*, 682 pp. New York: Dover Publications.
- Ita JJ and King SD (1998) The influence of thermodynamic formulation on simulations of subduction zone geometry and history. *Geophysical Research Letters* 25: 1463–1466.
- Jarvis GT and McKenzie DP (1980) Convection in a compressible fluid with infinite Prandtl number. *Journal of Fluid Mechanics* 96: 515–583.
- Kameyama MC and Yuen DA (2006) 3-D convection studies on the thermal state of the lower mantle with post perovskite transition. *Geophysical Research Letters* 33 (doi:10.1029/2006GL025744).
- Kageyama A and Sato T (2004) The 'Yin and Yang Grid': An overset grid in spherical geometry. *Geochemistry Geophysics Geosystem* 5(9): Q09005.
- Karato S and Wu P (1993) Rheology of the upper mantle: A synthesis. *Science* 260: 771–778.
- Kellogg LH, Hager BH, and van der Hilst RD (1999) Compositional stratification in the deep mantle. *Science* 283: 1881–1884.
- Kellogg LH (1992) Mixing in the mantle. *Annual Review of Earth and Space Sciences* 20: 365–388.
- King SD, Gable CW, and Weinstein SA (1992) Models of convection-driven tectonic plates: A comparison of methods and results. *Geophysical Journal International* 109: 481–487.
- King SD, Raefsky A, and Hager BH (1990) ConMan: Vectorizing a finite element code for incompressible two-dimensional convection in the Earth's mantle. *Physics of the Earth and Planetary Interiors* 59: 195–207.
- King SD and Hager BH (1990) The relationship between plate velocity and trench viscosity in Newtonian and power-law subduction calculations. *Geophysical Research Letters* 17: 2409–2412.
- King SD, Lowman JP, and Gable CW (2002) Episodic tectonic plate reorganizations driven by mantle convection. *Earth and Planetary Science Letters* 203: 83–91.
- Komatitsch D and Tromp J (1999) Introduction to the spectral element method for three-dimensional seismic wave propagation. *Geophysical Journal International* 139: 806–822.
- Kowalik Z and Murty TS (1993) *Numerical Modeling of Ocean Dynamics*, 481 pp. Toh Tuck Link, Singapore: World Scientific Publishing.
- Kuang W and Bloxham J (1999) Numerical modeling of magnetohydrodynamic convection in a rapidly rotating spherical shell: Weak and strong field dynamo action. *Journal of Computational Physics* 153: 51–81.
- Larsen TB, Yuen DA, Moser J, and Fornberg B (1997) A higher-order finite-difference method applied to large Rayleigh number mantle convection. *Geophysical and Astrophysical Fluid Dynamics* 84: 53–83.
- Lenardic A and Kaula WM (1993) A numerical treatment of geodynamic viscous flow problems involving the advection of material interfaces. *Journal of Geophysical Research* 98: 8243–8269.
- Lynch DR (2005) *Numerical Partial Differential Equations for Environmental Scientists and Engineers: A First Practical Course*, 388 pp. Berlin: Springer Verlag.
- Machetel Ph, Rabinowicz M, and Bernadet P (1986) Three-dimensional convection in spherical shells. *Geophysical and Astrophysical Fluid Dynamics* 37: 57–84.
- Maday Y and Patera A (1989) Spectral -element methods for the incompressible Navier-Stokes equations. In: Noor A and Oden J (eds.) *State of the Art Survey in Computational Mechanics*, pp. 71–143. New York: ASME.
- Malevsky AV (1996) Spline-characteristic method for simulation of convective turbulence. *Journal of Computational Physics* 123: 466–475.

- Malevsky AV and Yuen DA (1991) Characteristics-based methods applied to infinite Prandtl number thermal convection in the hard turbulent regime. *Physics Fluids A* 3(9): 2105–2115.
- Malevsky AV and Yuen DA (1993) Plume structures in the hard-turbulent regime of three-dimensional infinite Prandtl number convection. *Geophysical Research Letters* 20: 383–386.
- McKenzie DP, Roberts JM, and Weiss NO (1974) Convection in the Earth's mantle: Towards a numerical solution. *Journal of Fluid Mechanics* 62: 465–538.
- McNamara AK and Zhong S (2004) Thermochemical structures within a spherical mantle: Superplumes or piles? *Journal of Geophysical Research* 109: B07402 (doi:10.1029/2003JB002847).
- Monnereau M and Yuen DA (2002) How flat is the lower-mantle temperature gradient? *Earth and Planetary Science Letters* 202: 171–183.
- Moresi LN, Dufour F, and Muhlhaus H-B (2003) A Lagrangian integration point finite element method for large deformation modeling of viscoelastic geomaterials. *Journal of Computational Physics* 184: 476–497.
- Moresi LN and Solomatov VS (1998) Mantle convection with a brittle lithosphere: Thoughts on the global tectonic styles of the Earth and Venus. *Geophysical Journal International* 133: 669–682.
- Moresi LN and Solomatov VS (1995) Numerical investigation of 2D convection with extremely large viscosity variation. *Physics of Fluids* 9: 2154–2164.
- Moresi L and Gurnis M (1996) Constraints on the lateral strength of slabs from three-dimensional dynamic flow models. *Earth and Planetary Science Letters* 138: 15–28.
- Moresi LN, Zhong S, and Gurnis M (1996) The accuracy of finite element solutions of Stokes' flow with strongly varying viscosity. *Physics of the Earth and Planetary Interiors* 97: 83–94.
- Murakami M, Hirose K, Kawamura K, Sata N, and Ohishi Y (2004) Post-perovskite phase transition in MgSiO<sub>3</sub>. *Science* 304: 855–858.
- Ogawa M, Schubert G, and Zebib A (1991) Numerical simulations of 3-dimensional thermal convection in a fluid with strongly temperature-dependent viscosity. *Journal of Fluid Mechanics* 233: 299–328.
- Ohno N, Kageyama A, and Kusano K (in press) Virtual reality visualization by CAVE with VFIVE and VTK. *Journal of Plasma Physics*.
- Oosterlee CW and Gaspar-Lorenz FJ (2006) Multigrid methods for the Stokes system. *Computing in Science and Engineering* 8(6): 34–43.
- Osher S and Fedkiw RP (2003) *Level Set Methods and Dynamic Implicit Surfaces*, 275 pp. Berlin: Springer Verlag.
- Pantakar SV (1980) *Numerical Heat Transfer and Fluid Flow*. New York: Hemisphere Publishing Corporation.
- Pantakar SV and Spalding DB (1972) A calculation procedure for heat, mass and momentum transfer in three-dimensional parabolic flows. *International Journal of Heat and Mass Transfer* 15: 1787–2000.
- Parmentier EM and Sotin C (2000) Three-dimensional numerical experiments on thermal convection in a very viscous fluid: Implications for the dynamics of a thermal boundary layer at high Rayleigh number. *Physics of Fluids* 12: 609–617.
- Parmentier EM, Turcotte DL, and Torrance KE (1976) Studies of finite amplitude non-Newtonian thermal convection with application to convection in the Earth's mantle. *Journal of Geophysical Research* 81: 1839–1846.
- Parmentier EM, Turcotte DL, and Torrance KE (1975) Numerical experiments on the structure of mantle plumes. *Journal of Geophysical Research* 80: 4417–4425.
- Peyret R and Taylor TD (1983) *Computational Methods for Fluid Flow*, 350 pp. Berlin: Springer Verlag.
- Press WH, Flannery BP, Teukolsky SA, and Vetterling WA (1992) *Numerical Recipes in FORTRAN*. New York: Cambridge University Press.
- Ramage A and Wathen AJ (1994) Iterative solution techniques for the Stokes and Navier-Stokes equations. *International Journal of Numerical Methods in Fluids* 19: 67–83.
- Ratcliff JT, Schubert G, and Zebib A (1996) Steady tetrahedral and cubic patterns of spherical-shell convection with temperature-dependent viscosity. *Journal of Geophysical Research* 101: 25 473–25 484.
- Richter FM (1973) Finite amplitude convection through a phase boundary. *Geophysical Journal of the Royal Astronomical Society* 35: 265–276.
- Richtmeyer RD and Morton KW (1967) *Difference Methods for Initial Value Problems*, 405 pp. New York: Interscience Publishers.
- Rudolf M, Gerya TV, Yuen DA, and De Rosier S (2004) Visualization of multiscale dynamics of hydrous cold plumes at subduction zones. *Visual Geosciences* 9: 59–71.
- Saad Y and Schultz MH (1986) GMRES: A generalized minimal residual algorithm for solving nonsymmetric linear systems. *SIAM Journal on Scientific Statistical Computing* 7: 856–869.
- Schmalholz SM, Podladchikov YY, and Schmid DW (2001) A spectral/finite-difference for simulating large deformations of heterogeneous, viscoelastic materials. *Geophysical Journal International* 145: 199–219.
- Schott B and Schmeling H (1998) Delamination and detachment of a lithospheric root. *Tectonophysics* 296: 225–247.
- Schubert G, Turcotte DL, and Olson P (2001) *Mantle Convection in the Earth and Planets*. Cambridge, UK: Cambridge University Press.
- Schubert G, Yuen DA, and Turcotte DL (1975) Role of phase transitions in a dynamic mantle. *Geophysical Journal of the Royal Astronomical Society* 42: 705–735.
- Smolarkiewicz PK (1983) A simple positive definite advection transport algorithm with small implicit diffusion. *Monthly Weather Review* 111: 479–489.
- Smolarkiewicz PK (1984) A fully multidimensional positive definite advection scheme with small implicit diffusion. *Journal of Computational Physics* 54: 325–339.
- Spalding DB (1972) A novel finite difference formulation for differential expressions involving both first and second derivatives. *International Journal of Numerical Methods in Engineering* 4: 551–559.
- Spiegelman M and Katz RF (2006) A semi-Lagrangian Crank-Nicolson algorithm for the numerical solution of advection-diffusion problems. *Geochemistry, Geophysics, Geosystems* 7 (doi:10.1029/2005GC001073).
- Stemmer K, Harder H, and Hansen U (2006) A new method to simulate convection with strongly temperature-dependent and pressure-dependent viscosity in a spherical shell: Applications to the Earth's mantle. *Physics of the Earth and Planetary Interiors* 157: 223–249.
- Sulsky D, Chen Z, and Schreyer HL (1994) A particle method for history-dependent materials. *Computational Methods in Applied Mechanics and Engineering* 118: 179–196.
- Tackley PJ (2000) Self-consistent generation of tectonic plates in time-dependent, three-dimensional mantle convection simulations. Part 1: Pseudoplastic yielding. *Geochemistry Geophysics Geosystems* 1(8) (doi:10.1029/2000GC000043).
- Tackley PJ (1998a) Three-dimensional simulations of mantle convection with a thermo-chemical basal boundary layer: D'. In: Gurnis M (ed.) *The Core-Mantle Region*, pp. 231–253. Washington, DC: AGU.

- Tackley PJ (1998b) Self-consistent generation of tectonic plates in three-dimensional mantle convection. *Earth and Planetary Science Letters* 157: 9–22.
- Tackley PJ (1994) *Three-Dimensional Models of Mantle Convection: Influence of Phase Transitions and Temperature-Dependent Viscosity*. PhD Thesis, California Institute of Technology, Pasadena, CA.
- Tackley PJ (1993) Effects of strongly temperature-dependent viscosity on time-dependent, 3-dimensional models of mantle convection. *Geophysical Research Letters* 20: 2187–2190.
- Tackley PJ and King SD (2003) Testing the tracer ratio method for modeling active compositional fields in mantle convection simulations. *Geochemistry Geophysics Geosystems* 4 (doi:10.1029/2001GC000214).
- Tackley PJ, Stevenson DJ, Glatzmeir GA, and Schubert G (1993) Effects of an endothermic phase transition at 670 km depth on spherical mantle convection. *Nature* 361: 137–160.
- Torrence KE and Turcotte DL (1971) Thermal convection with large viscosity variations. *Journal of Fluid Mechanics* 47: 113–125.
- Travis BJ, Olson P, and Schubert G (1990) The transition from two-dimensional to three-dimensional planforms in infinite-Prandtl-number thermal convection. *Journal of Fluid Mechanics* 216: 71–92.
- Trompert RA and Hansen U (1998) Mantle convection simulations with rheologies that generate plate-like behavior. *Nature* 395: 686–688.
- Trompert RA and Hansen U (1996) The application of a finite-volume multigrid method to 3-dimensional flow problems in a highly viscous fluid with a variable viscosity. *Geophysical and Astrophysical Fluid Dynamics* 83: 261–291.
- Trottenberg U, Oosterlee C, and Schueller A (2001) *Multigrid*, 631 pp. Orlando, FL: Academic Press.
- Turcotte DL, Torrance KE, and Hsui AT (1973) Convection in the Earth's mantle in Methods. In: Bolt BA (ed.) *Computational Physics*, vol. 13, pp. 431–454. New York: Academic Press.
- van den Berg AP, van Keeken PE, and Yuen DA (1993) The effects of a composite non-Newtonian and Newtonian rheology on mantle convection. *Geophysical Journal International* 115: 62–78.
- van Keeken PE and Zhong S (1999) Mixing in a 3D spherical model of present-day mantle convection. *Earth and Planetary Science Letters* 171: 533–547.
- van Keeken PE, King SD, Schmeling H, Christensen UR, Neumeister D, and Doin M-P (1997) A comparison of methods for the modeling of thermochemical convection. *Journal of Geophysical Research* 102: 22477–22496.
- Verfurth R (1984) A combined conjugate gradient-multigrid algorithm for the numerical solution of the Stokes problem. *IMA Journal of Numerical Analysis* 4: 441–455.
- Weinberg RF and Schmeling H (1992) Polydiapirs: Multi-wavelength gravity structures. *Journal of Structural Geology* 14: 425–436.
- Yavneh I (2006) Why multigrid methods are so efficient? *Computing in Science and Engineering* 8: 12–23.
- Yoshida M and Kageyama A (2004) Application of the Yin-Yang grid to a thermal convection of a Boussinesq fluid with infinite Prandtl number in a three-dimensional spherical shell. *Geophysical Research Letters* 31: doi:10.1029/2004GL019970.
- Yuen DA, Balachandar S, and Hansen U (2000) Modelling mantle convection: A significant challenge in geophysical fluid dynamics. In: Fox PA and Kerr RM (eds.) *Geophysical and Astrophysical Convection* pp. 257–294.
- Zhang S and Christensen U (1993) Some effects of lateral viscosity variations on geoid and surface velocities induced by density anomalies in the mantle. *Geophysical Journal International* 114: 531–547.
- Zhang S and Yuen DA (1995) The influences of lower mantle viscosity stratification on 3-D spherical-shell mantle convection. *Earth and Planetary Science Letters* 132: 157–166.
- Zhang S and Yuen DA (1996a) Various influences on plumes and dynamics in time-dependent, compressible, mantle convection in 3-D spherical shell. *Physics of the Earth and Planetary Interiors* 94: 241–267.
- Zhang S and Yuen DA (1996b) Intense local toroidal motion generated by variable viscosity compressible convection in 3-D spherical shell. *Geophysical Research Letters* 23: 3135–3138.
- Zhong S (2006) Constraints on thermochemical convection of the mantle from plume heat flux, plume excess temperature and upper mantle temperature. *Journal of Geophysical Research* 111: B04409 (doi:10.1029/2005JB003972).
- Zhong S (2005) Dynamics of thermal plumes in 3D isoviscous thermal convection. *Geophysical Journal International* 154(162): 289–300.
- Zhong S and Hager BH (2003) Entrainment of a dense layer by thermal plumes. *Geophysical Journal International* 154: 666–676.
- Zhong S, Zuber MT, Moresi LN, and Gurnis M (2000) Role of temperature dependent viscosity and surface plates in spherical shell models of mantle convection. *Journal of Geophysical Research* 105: 11063–11082.
- Zhong S, Gurnis M, and Moresi LN (1998) The role of faults, nonlinear rheology, and viscosity structure in generating plates from instantaneous mantle flow models. *Journal of Geophysical Research* 103: 15255–15268.
- Zhong S and Gurnis M (1994) The role of plates and temperature-dependent viscosity in phase change dynamics. *Journal of Geophysical Research* 99: 15903–15917.
- Zienkiewicz OC, Taylor RL, and Zhu JZ (2005) *The Finite Element Method: Its Basis and Fundamentals* 6th edn. Woburn, MA: Butterworth and Heinemann.

## Relevant Websites

<http://www.geodynamics.org> – Computational Infrastructure for Geodynamics.

<http://www.lcse.umn.edu> – Laboratory for Computational Science and Engineering, University of Minnesota.